AD-A193 367 AN INVESTIGATION OF ATMOSPHERIC DYNAMICS THROUGH THEIR EFFECTS ON MESOSPH..(U) CINCINNATI UNIV OH DEPT OF PHYSICS T TUAN 23 MAR 87 AFGL-TR-87-0263 1/2

UNCLASSIFIED F19628-83-K-0026 F/G 4/1 NL

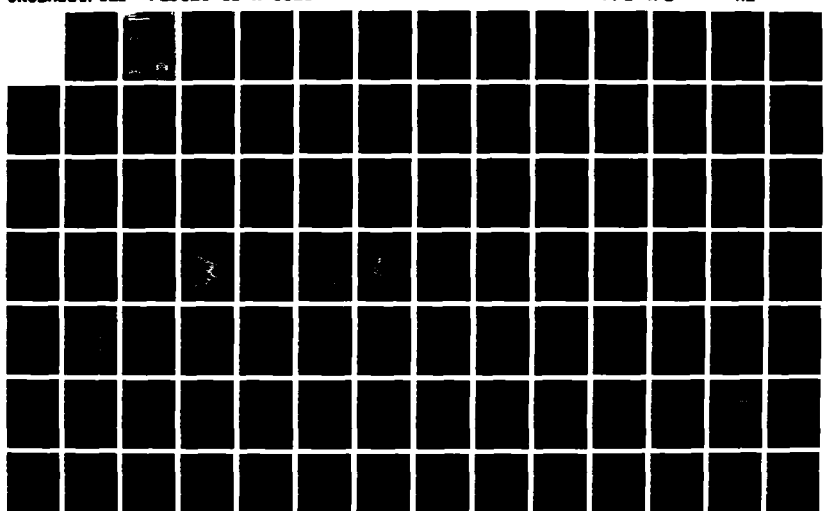

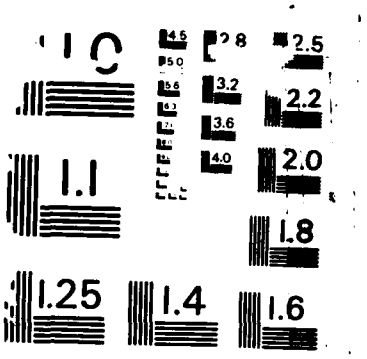

[redacted] OF GEOMAGNETIC [redacted]
[redacted] EFFECTS ON AURORAL OPTICAL EMISSION

Tai-Fu Tuan

University of Cincinnati
Physics Department
Cincinnati, Ohio 45221

23 March 1987

Final Report
1 September 1983 - February 28, 1987

AIR FORCE GEOPHYSICS LABORATORY
AIR FORCE SYSTEMS COMMAND
UNITED STATES AIR FORCE
HANSCOM AFB, MASSACHUSETTS 01731

Unclassified
SECURITY CLASSIFICATION OF THIS PAGE

REPORT DOCUMENTATION PAGE

1a. REPORT SECURITY CLASSIFICATION: Unclassified	1b. RESTRICTIVE MARKINGS
2a. SECURITY CLASSIFICATION AUTHORITY	3. DISTRIBUTION/AVAILABILITY OF REPORT: Approved for public release; Distribution unlimited
2b. DECLASSIFICATION/DOWNGRADING SCHEDULE	
4. PERFORMING ORGANIZATION REPORT NUMBER(S)	5. MONITORING ORGANIZATION REPORT NUMBER(S): AFGL-TR-87-0263
6a. NAME OF PERFORMING ORGANIZATION: University of Cincinnati; 6b. OFFICE SYMBOL (If applicable)	7a. NAME OF MONITORING ORGANIZATION: Air Force Geophysics Laboratory
6c. ADDRESS (City, State, and ZIP Code): Physics Department, Cincinnati, Ohio 45221	7b. ADDRESS (City, State, and ZIP Code): Hanscom AFB, Massachusetts 01731-5000
8a. NAME OF FUNDING/SPONSORING ORGANIZATION; 8b. OFFICE SYMBOL (If applicable)	9. PROCUREMENT INSTRUMENT IDENTIFICATION NUMBER: F19628-83-K-0026
8c. ADDRESS (City, State, and ZIP Code)	10. SOURCE OF FUNDING NUMBERS

PROGRAM ELEMENT NO.	PROJECT NO.	TASK NO.	WORK UNIT ACCESSION NO
61102F	2310	G5	AB

11. TITLE (Include Security Classification): An Investigation of Atmospheric Dynamics Through Their Effects on Mesospheric Optical Emission

12. PERSONAL AUTHOR(S): Tai-Fu Tuan

13a. TYPE OF REPORT	13b. TIME COVERED	14. DATE OF REPORT (Year, Month, Day)	15. PAGE COUNT
FINAL REPORT	FROM 9/1/83 TO 2/28/87	1987 March 23	100

16. SUPPLEMENTARY NOTATION

17. COSATI CODES		
FIELD	GROUP	SUB-GROUP

18. SUBJECT TERMS (Continue on reverse if necessary and identify by block number)
Atmospheric gravity waves; Ducting; Airglow; Wave filtering; Mesosphere; Hydroxyl airglow (OVER)

19. ABSTRACT (Continue on reverse if necessary and identify by block number)

Research is described on various aspects of the dynamics of atmospheric gravity waves and their effect on mesospheric airglow emissions, in particular hydroxyl emission. Simultaneous observations of mesospheric optical emissions obtained during the MAPSTAR campaign at Boot Lake, Colorado, are analyzed using maximum-entropy spectral analysis and other methods. The velocity-field profiles extracted from this data are compared

20. DISTRIBUTION/AVAILABILITY OF ABSTRACT	21. ABSTRACT SECURITY CLASSIFICATION
☐ UNCLASSIFIED/UNLIMITED ☐ SAME AS RPT ☐ DTIC USERS	Unclassified

22a. NAME OF RESPONSIBLE INDIVIDUAL	22b. TELEPHONE (Include Area Code)	22c. OFFICE SYMBOL
Arthur Corman		AFGL/LSI

DD FORM 1473, 84 MAR — 83 APR edition may be used until exhausted. All other editions are obsolete.

SECURITY CLASSIFICATION OF THIS PAGE
Unclassified

CONT OF BLOCK 18:

Fully guided waves
Spectral analysis
Gravity-wave models

CONT OF BLOCK 19:

with gravity-wave models based on a realistic non-isothermal background atmosphere. This work enables one to make direct comparisons between airglow data and radar-determined wind profiles. A program aimed at investigating small temporal and spatial scale airglow fluctuations is outlined, and the simultaneous ducting and filtering of short-period gravity waves by an atmosphere with a non-isothermal temperature profile is modeled theoretically. It is shown that waves from lower-atmospheric or terrestrial sources with group velocity upward are reflected at the altitude where the wave frequency becomes equal to the local Brunt-Vaisala frequency. This filters out the shorter-period waves, preventing them from reaching higher altitudes and, in conjunction with the ground boundary condition, results in a set of fully guided modes, whose frequency dispersion is investigated.

Final Report

Contents

(I) INTRODUCTION

The research program undertaken for this report is divided into three parts. In the first part we analyze the simultaneous observations of different mesospheric optical emissions within the ongoing MAPSTAR program in which we have also had some participation in the field work. We then in the second part decompose these observations into their monochromatic Fourier components and match them with COSPAR-based gravity wave models to obtain various wind profiles from which other atmospheric parameters (e.g. the kinetic energy density) can be derived. The results can be compared with the more direct simultaneous observations of wind profiles from MST radar, which will form part of the future MAPSTAR program. Such comparisons can connect the ground-based optical emission data with the simultaneously observed radar data and provide information on gravity wave models as well as on the chemistry and dynamics of wave-induced airglow fluctuations. In this report, we shall present the steps which can allow us to extract the velocity fields from the observed airglow using the purely dynamical model of Hatfield et al (1981). A proper chemical-dynamical model is under development and the methods presented here can be immediately adapted to the more fully developed model.

In part three we begin an investigation into the behavior of small scale spatial-temporal airglow fluctuations induced by gravity waves. The investigation is of intrinsic physical interest in that it examines a simultaneous ducting and filtering mechanism for small-period gravity waves which are restricted to lower height levels, leaving the longer period

waves to penetrate to higher altitudes. In terms of airglow, such a result can imply an overall greater probability of finding small scale spatial-temporal mesospheric airglow fluctuations occurring simultaneously with larger scale ionospheric airglow fluctuations. This applies only to lower altitude sources and some of the medium-scale T.I.D.'s. The problem should also be of interest to the Air Force, since it deals, in particular, with small scale infrared fluctuations.

For the first part, we shall deal specifically with the observations and analyses of the 7300Å OH bands, the 5577Å OI green line, as well as some radiometric data with a 1.53 μm window. The observations have been made at Colorado (Bootlake), Wyoming (Jelm) and New Mexico (Capilla Peak) by Peterson, Pendleton and Lin, as part of the MAPSTAR campaign of 1984 and most of the observations were taken during a period from May 20 to July 3, 1984. The reason is that for only these two particular days we have both the radiometric and the photometric data as well as even some interesting interferometric data which are unfortunately not so easily usable because of the relatively short and interrupted data base. There is also the additional reason that day 176 represents a typically active day while day 182 represents a very active day. Actually, both from the observed fluctuations and from the computation of percentage fluctuations day 180 (June 27, 1984) is unquestionably the most disturbed day of the 1984 campaign, but since we do not have the radiometric data for day 180 for a more complete analyses, we shall work with day 182 as the next best example.

The analyses will be divided into three categories:

(1) Phase Correlation

(2) Frequency Correlation

(3) Comparison of percentage r.m.s. fluctuations

For (1) we shall superimpose photometric and radiometric observations made during the same time period and at the same location to establish any phase correlation between different spectral lines. Cross covariances will also be computed to lend more quantitative support to the simple visual comparisons. As we shall see, the phase relationships can be very complicated depending on factors ranging from the nature and location of the sources, the geometry of the observation point relative to the source, to the shape of the profiles of the ambient atmospheric constituents which produce these optical emissions (Thome (1968), Porter & Tuan (1974), Chiu & Ching (1978) & Hatfield et al (1981)).

For (2) we shall use four different kinds of power spectrum analyses; the maximum entropy (M.E.); the Blackman and Tukey (B.T.); the modified periodograms and the M-Step Difference Filter on M.E. We shall base our analysis primarily on the M.E. and use the others merely as a check since the M.E. has the best resolution for the size of our data base with the Nyquist frequency corresponding to a period of one minute which is well below the smallest period we seek (about 5 min.). The results of the analyses will then be listed (after subtracting the Window affects) with

the most prominent periodicity underlined. We shall also list the common periodicity between different spectral lines observed at the same location and time. Unlike the comparison of phase which depends so much on the shape of the ambient undisturbed background intensity distribution, the frequencies are independent of the shape of the ambient background and common frequencies may be expected to occur even if there does not appear to be a definite phase relationship.

For (3) we shall list the percentage r.m.s. fluctuations in the air glow averaged over 60, 30, 15, 10 and 5 minutes. Since there is no good unique method to determine the general trending which may occur for reasons other than purely atmospheric dynamics, we have decided to average over the above sets of different time intervals. The average over the shorter periods will automatically include trending without the necessity to determine the cause for such trending. The averaging over different time intervals will also allow us to evaluate the relative importance of small period oscillations as compared to the longer period oscillations. For instance, the long period fluctuations of one day may be more significant than another, but the short period fluctuations may be precisely the reverse. The comparison of r.m.s. percentage fluctuations will also provide us with a more quantitative means of picking out the most active day as well as the least active day. Lastly, just as the phase relationship between different spectral lines depend on the shape of the ambient profile, the magnitude of the response of the various "minor" atmospheric constituents (which produce the atmospheric emission) to an incoming gravity wave also depends on the shape of the ambient density

profile. In general, the response is much greater if the vertical density gradients is positive, i.e. opposite to the vertical density gradients of the major atmospheric constituents. Thus, fluctuations in the optical emission may well be greater owing to the peculiarities of its ambient emission profile. If all or most of the emission profile has a layered structure with a very narrow half-width, then the very large vertical gradients would produce a rather large fluctuation. This means that the percentage r.m.s. fluctuation would also tend to be more significant.

The second part deals with the extraction of velocity field profiles from the observed data. We have decomposed the observed airglow data for June 23 and June 29, 1984 into their Fourier components from FFT power spectrum analyses. For the present case we cannot use the Max. entropy method for the simple reason that it does not lend itself readily for Fourier decomposition. We will instead use the fast Fourier with a Haming window. Since the undisturbed background emission is a very slowly varying function of time, the background will be approximated by its time-averaged value. In this way we can obtain the percentage fluctuation for each Fourier component corresponding to a particular frequency. We can then use the theoretical computations of the fluctuations of airglow (Hatfield et al (1981)) (Modified to include the fluctuation of the chemical rate coefficient from temperature waves) produced by COSPAR gravity-wave models for the same fixed frequency and adjust the amplitudes of the vertical and horizontal velocity wave components until the theoretically computed percentage fluctuation equals the observed fluctuation just mentioned. The

adjusted velocity wave components so obtained would give us the vertical and horizontal winds.

For part three we investigate the small scale spatial temporal airglow fluctuations produced by gravity waves. For this report we shall only consider a simple two-layer model plus a rigid ground boundary. We shall also be exclusively concerned with low-altitude sources which form an important contribution to the medium-scale T.I.D.'s. The two-layer model provides much of the basic physics without any extraneous complications. A much more detailed treatment using the COSPAR atmospheric model plus horizontal wind profiles as well as careful consideration of viscosity, non-linearity and dissipation is being worked out. So far, the two results differ mostly in qualitative details.

The basic physics rests on the fact that a gravity wave propagating upwards would reach height levels where the frequencies of its higher Fourier components (within the range of the Brunt frequencies) become equal to the local Brunt frequencies causing them to be reflected earthward, leaving only the Fourier components below the Brunt-frequency range to continue their upward propagation. The variation of the Brunt frequency curve with height would then serve as a filter which filters out the higher frequency components and allowing only the longer period Fourier components to propagate into the ionospheric regions. In the meantime, the higher frequency reflected components would, with the help of the ground boundary, form a complete set of fully guided modes for each frequency. We shall

investigate the frequency dispersion of the spectrums of fully guided modes within the context of a two-layer model as part three of this report.

(II) Observations & Data Analyses for 1984 MAPSTAR Program

(1) Phase Correlation

In general , we assume that the gravity wave is carried by the major atmospheric constituents. The response of the minor constituents (which produce the airglow) through collisions with the major constituents depends on their vertical concentration gradients relative to the major constituents. If the minor constituent has a layered structure such as O which produce the 5577 OI or H and O_3 which produce the OH emissions, then there is a 180# phase change between the response at the bottom side and the top side of the layer with a continuous variation in the phase of the response in between (Thome, [1968], Testud & Francois (1971), Klostermeyer (1972 a,b) Porter and Tuan (1974), Dudis and Reber (1976) Chiu and Ching (1978), Hatfield, Tuan, and Silverman (1981)). In this section we shall consider the particular case of 5577 OI and 7900 A OH both observed at Jelm, Wyoming. Since what we observe is integrated along the line of sight, the actual phase of the integrated response depends therefore on the relative importance of the local response at different points along the line of sight. The situation is further complicated by the fact that we are not in general dealing with gravity waves with plane wave fronts and that the source for such waves may be either very close or some considerable distance away. As a result, we should not expect any definite

phase relationship between any two different types of airglow for different sources. We do expect definite phase relationship to exist for the very distant sources and the long-period gravity waves which produce the large-scale T.I.D.'s. A comparison of the density variations in H and O_3 with the density variation of the major atmospheric constituents reveal the 180# phase change between the bottom and top sides of the H and O_3 layers (Hatfield et al (1981)).

Fig. 1a shows the 5577 OI superimposed over the simultaneous OH observations for day 176 (June 23, 1984). In this particular case there does appear to be considerable correlation. The variations appear to be in phase. Since both the ambient 5577 OI and the 7900 OH have a layered structure, this result would have been expected for a relatively distant source.

Fig. 1b shows the phase correlation by a plot of the cross variance as a function of the lag time. The positive maxima centers at $s = -20$ which indicates that the 5577 OI and the 7900 OH are approximately out of phase by about 20 min. Both sums dropped off to zero at about 60 min. to either side of the center of the maxima showing a fundamental 4 hour period which agrees with the crossed power spectrum of the 5577 OI and the 7900 OH (dark line) in Fig. 1c. The latter shows a very high peak at frequency $f = .0038$ min.$^{-1}$ which also corresponds to approximately 4 hours.

Fig. 2a shows a plot of the same two spectral lines for day 180 (June 27, 1984). Here we should remark that even though we have not chosen this particular day for detailed analysis (there is no radiometric data for this day) we have decided to show it as the most active day (at least at Jelm, Wyoming) in the entire campaign. This is evident both from the observed data and from the computed percentage r.m.s. fluctuations. There does not appear to be any obvious phase relationship. An additional possibility exists where the relative strengths of different sources vary throughout the night so that phase correlation can also vary. The two curves can be in phase for part of the night and out of phase for the remainder of the night.

Fig. 2b shows the plot of the cross covariance as a function of lag time for June 27 (1984). The negative minima which centers again at $_s$ = -15 and indicates that the 5577 OI and the 7900 OH are out of phase by about 15 min. from purely 180# out of phase. The cross covariance goes to zero at about 55 min. from the center, giving us a fundamental period of about 220 min. The crossed power spectrum (Fig. 2c) shows a peak which centers at about 200^{-1} min. which is consistent with the crossed-covariance curve.

Fig. 3a shows the plot of the two spectral lines for day 182 (June 29, 1984). This was chosen as the most active day, although its r.m.s. fluctuations is only the second largest in the campaign. Once again, the phase correlation appears sporadic. A definite correlation appears to

exist beyond the 3rd hour of the observation. Before that time, one can perhaps make a case for some anti-correlation (i.e. 180# out of phase).

Since the phase correlation varies from approximately 180# out of phase to being approximately in phase, we should use a moving window of about 2 hour duration, or divide the night up into several parts. With a single fixed window for the entire night, the cross covariance (Fig. 3b) does not show much in the way of correlation. In general, for both of the very active days (June 27 & 29), it appears that phase correlation for the small period fluctuations appear to exist. For instance, on June 27, (Fig. 2a) considerable correlation exists for the 15 min. fluctuations at 67.5 min., 77 min., and 99 min. A phase shift begins to occur at about 2 hours and a sub-peak in the OH appear to be shifted by about 7.5 min. from the corresponding peak for OI. The phase shift appears to be further increased at 157.5 min. where the peak for OH appears to be shifted by about 14 min. For June 29 (Fig. 3a) the matching of subpeaks before 3 hours appear to be more difficult, although the OH and OI appear to be in phase after 3 hours.

(2) Frequency Correlation

Unlike phase correlation which depends on the many factors mentioned in the last section, the frequency correlation should be more readily established, since it is the independent variable and the response of the minor atmospheric constituents which produce the airglow must necessarily share some common frequency spectrum with the atmospheric disturbance in the major constituents.

As already mentioned in the Introduction, although we have used four different kinds of power-spectrum analyses, we shall rely primarily on the maximum entropy method. The following procedure will be adopted for each set of observations: (1) We eliminate the unwanted window together with its possible leakage produced by its finite data base. Here, although a number of papers exist which deal with the existence of the Window (Beamish (1977) Gasser (1974) Martin (1979), Wahbe (1968), Beamish and Priestly (1980), Ulrich (1972), Ulrych et al (1973), Ulrych and Bishop (1975)) for a maximum entropy analysis (it certainly does occur for the Fast Fourier method), we have found that it does exist even if there is relatively little leakage. To be safe, we also discard the higher harmonics corresponding to each window and shall refer to both as "background harmonics". In the event an exceptional prominent peak occurs close enough to one of the background harmonics so as to be indistinguishable, we check with the observed data to see if such a peak oscillation may indeed occur. If the check is positive, we identify it as a possible real oscillation: (2) We pick out all the other possible series whose fundamental is <u>not</u> a member of the background series. The difficulty lies in the higher frequencies where the members of the different series begin to merge and a member of one series may also appear to be a different member of another series: (3) For the very active and highly disturbed days, we check if any especially prominent high frequency peaks with periods in the range of 5-12 minutes may occur, since highly disturbed days may produce instability with this type of periodicity (Tuan et al (1979), Schoeberl et al, (1983)):

(4) For Highly disturbed days we also search for any possible subharmonics whose power peaks are related in a universal way (Feigenbaum (1983)).

For June 23, we have simultaneous observations of 5577 OI and 7300 A OH available for Wyoming as well as the 5577 OI and the Radiometric data at Colorado. Fig. 4a, 4b, and 4c show the observed 5577 data and the M.E. power spectrum analysis for this day. By replotting the higher frequencies on a larger scale one can show that after discarding the background series with its fundamental at 315 min., we obtain the following possible sets of series within the limits of resolution:

(1) T = 70, 18, 6.4, 5.9, 5.1 min.

(2) T = 30, 7.6, 6.1, 5.1

(3) T = 12.9, 6.4

(4) T = 9.4

The relatively prominent peaks (underlined) which do not seem to be higher harmonics of other series are 70, 30, 12.9 and 9.4 min. Thus, the analysis appears to show that there are long period oscillations of the order of 70 and 30 minutes with short period oscillations of the order of 12.9 and 9.4 minutes. Not shown are a group of peaks from 7 to 5 minutes. We would like to stress that all these peaks are very much higher than the required 2-4 times greater than the noise level. The two short-period oscillations of 12.9 min. and 9.4 min. are more prominent than many peaks immediately preceding them and do not appear to belong to members of any series.

For the 7900 A OH observed at nearly the same time, we have the following possibly real series:

(1) T = 37.5, 18.2, 12.0, 7.2 min.

(2) T = 26, 13.3, 9, 5.4

(3) T = 18.2

(4) T = 7.7

Fig. 5a, 5b, and 5c show respectively 7900 A OH and the M.E. analysis. Again, we discard the background series. The prominent peaks (underlined) are 37.5, for the large periods and 7.7 for the short periods. Again the 7.7 min. peak occurs as an isolated peak with many small peaks of lower frequency preceding it. Both observations show more peaks in the 70-80 and 30-40 min. range. Both show an 18 min. harmonic. Both show small period prominence in the 12-14 min. range as well as the 7-9 min. range. The real question here is how big a role does the interference of the background series play in either case. The background fundamental for the 5577 A has a period of 315 min., while the background fundamental for the 7900 A has a period of 300 min. Furthermore, the starting time is not exactly the same. We are presently examining the data with the same background fundamental and the same starting time.

For the 5577 A OI at Bootlake, Colorado, we obtain the following possible series:

T_1 = 21,5, 10, 6.8, 5.6

T_2 = 15.8, 7.9, 5.6

T_3 = 13.1, 6.8, 4.6

T_4 = 12, 5.6

The prominent peaks (Fig. 6a, 6b, 6c) appear quite strongly for the shorter period oscillations, particularly the 6.8 min. oscillation which stands out among the rest of the peaks. A relatively broad peak occurs at 50 min. (not listed above), but its height level is merely comparable to the 6.8 min. peak.

For the radiometric observations in the same day, the series are given by:

T_1 = 52, 23.9, 16.3, 8.9, 6.2, 4.7

T_2 = 34, 16.3, 8.9, 5.5

T_3 = 7.8

The observed data and the power spectrum analysis are given in Fig. 7a, 7b, 7c. The 8.9 and 7.8 min. peaks appear significant and are more prominent than nearby peaks. The total useful data base for both sets of Colorado results is about 3 hours. So we should be concerned only with the shorter period fluctuations for these data.

For the very active day (Day 182), we have simultaneous observations of 5577 A OI and 7900 A OH at Wyoming, 7300 A OH at New Mexico 5577 A OI and radiometry at Colorado. Fig. 8a, 8b and 8c show 5577 A OI and the M.E. analysis for this day. The length of data base for this day is 237.5 min. Again, after discarding the background series of frequencies, we obtain the

following:

(1) T = 79, 28, 12.8, 11.3, 5.6, 5.3, 4.4

(2) T = 36.5, 12.8, 5.3

(3) T = 17, 8.2, 5.6

(4) T = 5.6

The relatively prominent peaks occur at 79 min. (which is very close to the second harmonic of the background fundamental), 28 min. and 5.6 minutes. Although it is within our margin of resolution, the 28 minutes peak can easily itself be a fundamental and does not belong to the first series (series (1)). Unlike the active day the very active day shows a surprisingly prominent peak relative to other nearby peaks at 5.6 min.

Fig. 9a, 9b, and 9c show the respective results for 7900 A OH taken at Wyoming. The length of data base is 237.5 min. and the possibly real sets of series are:

(1) T = 158.3, 31.7, 17.6, 11.3, 5.3, 4.1

(2) T = 25

(3) T = 17.6, 9.1?

(4) T = 6.0

The interesting feature here is the big peak at T = 158.3 min.; almost exactly double the 79 min. peak for the 5577 A OI. Since T = 158.3 min. cannot be a harmonic of the background fundamental (237.5 min.), it lends

greater credibility to the possibility that the 79 min. peak is real. Once again we have a prominent short-period 6 min. peak.

Fig. 10a, 10b, and 10c show the results for the 7300 A OH observed at Capilla Peak. The length of data base is 240 min. The possibly real series are:

(1) T = 96, 25.3, 20, 10.9, 9.8, 7.5, 4.2

(2) T = 40, 20, 13.3, 9.8, 6.8, 5.8

(3) T = 15.5, 7.5

(4) T = 10.9, 5.5

There are a few split peaks. We have assumed that a 37 min. split peak is more likely to be about 40 min. Once again, there are prominent peaks relative to their immediate neighbors at 7.5 min. and 4.2 min.

Correlations between different data taken at the same location do appear to exist, although they do not seem to, from the raw data without the power spectrum analysis. Based on the very limited information, the very active day (Day 182) does appear to have more prominent short-period oscillations relative to their neighboring peaks as compared with the average active day (Day 176). Far more observations will have to be made before any real significance can be attached to this result.

Fig. 11a, 11b and 11c show the results for the 5577 A OI at Bootlake, Colorado. The useful length of data base here is about 5 hours and we see

that like Wyoming, there appears to be considerable activity. The following series may be obtained from the power spectrum analysis:

T_1 = 210, 26.3, 8.4, 7.5

T_2 = 57, 11.9, 9.4, 8.4, 6.3, 5.2

T_3 = 21.8, 10.4, 5.4

T_4 = 18.0, 6.1

T_5 = 15.4, 7.5

A rather prominent peak appears at 26.3 min. The higher peaks appear much smaller by comparison.

For the radiometric data (12a, 12b, 12c) at Bootlake, we obtain the following possible series:

T_1 = 221, 36.9, 20.1, 17.0, 8.5, 5.5, 4.5

T_2 = 60, 20.1, 15.5, 10.2, 8.5, 7.5, 5.9, 5.5

T_3 = 22.9, 11.5, 7.5, 4.5

The length of data base is about 5.5 hours. We have an especially prominent peak at 10.2 min.

In general, the power spectrum analysis for day 182 (June 29, 1984) appears to have less prominent small period (5-10 min.) peaks than day 176. This appears surprising in view of the fact that June 29, by most criteria,

is a more active day. Later, we will show that the r.m.s. fluctuations confirm this expectation.

Tables I, II, III, IV, V and VI show the common peak (peaks with similar periods) for different ranges in the oscillation periods. For day 176, the most common peaks appear in the short period ranges (Table V). The same is true for day 182, although for this day considerable common peaks appear in 11-20 min. range, (Table IV). For both days, there exists considerable less common peaks for the long period fluctuation, (Table I & II). One possible explanation is that the natural "bunching" together of higher harmonics at the short period end. However, this does not explain the profuse number of peaks in the 5-6 min. range. Although much more data is needed before any definite statement can be made, we believe that there may be a tendency for short period oscillations of the order of 4.5-7 min. to occur with greater frequency than other periodicities. We may add that this type of peaks occur without regard to location (i.e. irrespective of whether the observations were taken in Colorado, Wyoming or New Mexico). Some location bias seems to occur for the longer period fluctuations.

(3) Comparison of Fluctuation Magnitude

Just as the case for Phase correlations (Section I), the magnitude of the fluctuations also depends on the vertical density gradient of the unperturbed minor atmospheric constituent relative to the major atmospheric constituent (Porter & Tuan (1974), Dudis & Reber (1976), Chiu & Ching (1978)). In general, if the vertical density gradients of the minor

constituents which produce the airglow are opposite to the corresponding gradients of the major constituents which are presumed to carry the gravity wave (e.g. the bottom side of a layered structure in the minor constituents) the response tends to be large. The percentage fluctuations on the top side of the layered structure on the other hand would tend to be of the same order as the major constituents carrying the gravity wave.

In computing the r.m.s. fluctuation, one way is to put in a polynomial approximation to represent the average "quiet" background and then compute the average r.m.s. deviations from this "background". Rather than making this assumption, we have decided to compute the percentage r.m.s. fluctuation about the averages over 60, 30, 15, 10 and 5 min. intervals. The fluctuations computed over the 5 min. interval averages must only include the short period oscillation. In this way we do not have to specifically assume some kind of polynomial "background".

Table VII shows the percentage r.m.s. fluctuation for day 176 and 182. The checks indicate the day with clearly the greater fluctuation, whilst the checks with crosses indicate the day with the slightly to somewhat greater fluctuation. A glance at the Table would show that day 182 (June 29) is clearly the more active day. A second glance would show that whilst June 29 was clearly the more disturbed day in terms of long-period fluctuation, June 23 appears to have a very slight edge for the shorter-period fluctuations. Such a conclusion is consistent with the power spectrum analyses which seemed to show relatively more prominent short period peaks for June 23. The last row of Table VII shows the difference

in percentage fluctuation between the 2 days expressed as a percentage of the June 29 fluctuation percentage. With exceptions in one radiometric data at Colorado and one OI data at Wyoming, the difference in percentage fluctuation is clearly less for the shorter 10 to 5 min. periods. This means that the June 23 data showed relatively greater short-period fluctuations.

Table VIII shows the total r.m.s. percentage fluctuation. The averaging was made over the entire data base. The result shows a very high Colorado radiometric data fluctuation. Since this averaging includes the "quiet" background variations, one cannot make any meaningful more detailed analysis.

Table IX shows the percentage r.m.s. averages of all different data for each day as well as the percentage of the shorter period oscillations to the 60 min. oscillation. Clearly again June 23 has more significant short-period oscillations.

In Table X, we present a comparison of the percentage r.m.s. fluctuations for six days (from June 21 to June 29 inclusive) of the Wyoming 5577 OI and 7900 OH data. As already mentioned in the Introduction, day 180 appeared to be very active in Wyoming both from the observed data and from the computed r.m.s. fluctuations. Clearly, the column for June 27, Table X shows that the percentage r.m.s. fluctuation for this day is consistently the largest. The day we chose (June 29) as the most active is arguably the second most active.

The most interesting consistent result is that irrespective of whether the averaging was over 60, 30, 15, 10 or 5 min. intervals, the magnitude of the percentage r.m.s. fluctuation is consistently greater for the 5577 OI as compared with the 7900 OH. There is one exception for the 30 min. interval average on June 23 where the percentage r.m.s. fluctuation was slightly in favor of the 7900 OH. Assuming that there are no systematic errors or instrumental bias, we may conclude that for the 5577 OI, the bottom side of the atomic oxygen profile has a sharper vertical gradient as compared with the constituents which produce the 7900 OH, and that on the whole the 5577 OI profile is primarily concentrated over a narrower layer than say the 7900 OH.

A similar statement may be made about the radiometric data which seems to show from Table VII a consistent greater percentage fluctuation than either the 5577 OI or the 7900 OH.

(III) Extraction of Velocity Field Profiles From Airglow Observations

(1) FFT Decomposition of Observed Data

The observed optical emissions data may be Fourier decomposed in the following way:

$$Q(t) = Q_o(t) + \Delta Q(t)$$
$$= S_o + \Sigma \, (a_k \cos\omega_k t + b_k \sin\omega_k t) \qquad (1)$$

where Q_o = unperturbed background trend

ΔQ = fluctuations produced by gravity waves

S_o = time averaged unperturbed trend (quite close to Q_o)

a_k, b_k = Fourier coefficients in the decomposition of $\Delta Q(t)$

ω_k = frequency of the kth harmonic in the decomposition.

We may hence write,

$$\frac{\Delta Q(t,\omega_k)}{Q_o} - \frac{a_k \cos\omega_k t + b_k \sin\omega_k t}{S_o} \qquad (2)$$

where $\Delta Q(t,\omega_k)$ is the observed fluctuation for each frequency, ω_k. Since most available gravity-wave models are essentially monochromatic models, we use a model for each frequency, ω_k.

To determine the gravity wave amplitude which will give the observed fluctuation given by (2), we consider the gravity-wave induced fluctuations in airglow. To be specific, we consider observation along the zenith for the special case of OH emissions. We consider the following reactions:

$$H + O_3 \rightarrow OH^* + O_2 \qquad (3)$$

$$OH^* \rightarrow OH + h\nu \qquad (4)$$

If k is the rate coefficient for (3) and ξ is the efficiency of photon emission per OH molecule, we may write:

$$I = \xi \Sigma k[O_3][H] \qquad (5)$$

Where I is the total volume emission rate. We may write,

$$I = I_o + \Delta I \tag{6}$$

Where I_o is the unperturbed volume emission rate and ΔI is the perturbed emission rate produced by the gravity wave.

$$\Delta I = \zeta \Sigma k_o [O_3]_o [H]_o \left[\frac{\tilde{\Delta k}}{k_o} + \frac{\Delta[\tilde{O_3}]}{[O_3]_o} + \frac{\Delta[\tilde{H}]}{[H]_o} \right] \tag{7}$$

where $\Delta[\tilde{O_3}]$, $\Delta[\tilde{H}]$ and $\Delta\tilde{k}$ are the fluctuations produced by the gravity waves. In (7) we have neglected the non-linear terms for simplicity. Throughout this report we will use not only linearized gravity wave models, but also linearized response.

Through assuming a horizontally stratified atmosphere,

$$\begin{aligned} \Delta[\tilde{O_3}] &= \Delta[O_3] e^{i(\omega t - k_x x)} \\ \Delta[\tilde{H}] &= \Delta[H] e^{i(\omega t - k_x x)} \\ \Delta\tilde{k} &= \Delta k e^{i(\omega t - k_x x)} \end{aligned} \tag{8}$$

where $\Delta[O_3]$, $\Delta[H]$ and Δk on the right-hand side depend only on z.

Substituting (8) into (7) and integrating over z (the vertical column) we obtain,

$$\frac{\Delta Q_T(t,\omega)}{Q_{oT}} = \frac{\Sigma \int \zeta\, k_o [O_3]_o [H]_o \left\{ \frac{\Delta k}{k_o} + \frac{\Delta[O_3]}{[O_3]_o} + \frac{\Delta[H]}{[H]_o} \right\} dz e^{i(\omega t - k_x x)}}{\Sigma \int \zeta\, k_o [O_3]_o [H]_o dz} \tag{9}$$

If we make the observation at $x = x_o$ and take the real part of (9), we obtain,

$$\Sigma \int \varsigma \; k_o[o_3]_o[H]_o \left\{ \frac{\Delta k}{k_o} + \frac{\Delta[o_3]}{[o_3]_o} + \frac{\Delta[H]}{[H]_o} \right\} dz$$

$$Re\left[\frac{\Delta Q_T(t,\omega_k)}{Q_{oT}}\right] = \frac{x\ (\cos\omega_k t \cos k_x x_o + \sin\omega_k t \sin k_x x_o)}{\Sigma \int \varsigma \; k_o[o_3]_o[H]_o dz} \qquad (10)$$

Again, using linearized response and neglecting chemistry, we may write,

$$\frac{\Delta[x]}{[x]_o} = \frac{V_{phx}}{c^2} \Delta u + \frac{i}{\omega} \left\{ \frac{1}{N_o} \frac{dN_o}{dz} + \frac{g}{c^2} \right\} \Delta w \qquad (11)$$

where [x] is an arbitrary species. Here we also note that (11) is real, since Δw is pure imaginary. The rate coefficient can be expressed in terms of temperature, (Jackman & McPeters (1985)) and is given by:

$$k = Ae^{-\left(\frac{B}{T}\right)} \qquad (12)$$

from (12) we obtain

$$\frac{\Delta k}{k_o} = \left(\frac{B}{T_o}\right)\left(\frac{\Delta T}{T_o}\right) \qquad (13)$$

and it is easy to show that

$$\frac{\Delta T}{T_o} = (\gamma - 1)\frac{\omega}{K_x c^2} \Delta u + \frac{i}{g} \frac{\omega_b^2}{\omega} \Delta w \qquad (14)$$

Thus all the ratios in the bracket of (7) can be expressed in terms of a linear combination of Δu and Δw.

(2) Matching of decomposed monochromatic data with monochromatic gravity-wave models

If we define a standard velocity field by,

$$\begin{aligned} \Delta u(z, \omega_k) &= \alpha_k \Delta u_s (z, \omega_k) \\ \Delta w (z, \omega_k) &= \alpha_k \Delta w_s (z, \omega_k) \end{aligned} \tag{15}$$

We may then adjust α_k so that

$$\frac{\Delta Q(t, \omega_K)}{Q_o} = \alpha_k \, \mathrm{Re} \left[\frac{\Delta Q_T (t, \omega_k)}{Q_{oT}} \right] \tag{16}$$

where $\Delta Q_T(t, \omega_k)$ now contains Δu_s and Δw_s only. From comparing (16) with (10) and (2), we obtain

$$\begin{aligned} a_k &= \alpha_K \Delta J_s \cos k_x x_o \left(\frac{S_o}{Q_{oT}} \right) \\ b_k &= \alpha_K \Delta J_s \sin k_x x_o \left(\frac{S_o}{Q_{oT}} \right) \end{aligned} \tag{17}$$

In (17) we know a_k and b_k from the Fourier decomposition of observed data and we also know k_x if we know the horizontal phase velocity. Thus,

$$\tan k_x x_o = \frac{b_k}{a_k}$$

$$\alpha_k = \frac{a_k Q_{\sigma T}}{S_o \Delta J_s \cos k_x x_o} = \frac{b_k Q_{\sigma T}}{S_o \Delta J_s \sin k_x x_o} \tag{18}$$

Once α_k is determined, we can determine the velocity fields from equation (15).

To get a feel for how this can be used, we shall assume that the observations are taken along the zenith. We will use the standard atmospheric models of Yu et al (1980) which is based on COSPAR. We will work with the 7900 OH for our observed data since for this data the variation in $Q_o(t)$ for June 23 and 29 of 1984 is quite small and may be replaced by the time-averaged constant, S_o, given by equation (1). The results for June 23, 1984 at periods of 150 min. and 37.5 min. are listed in Tables XI (a) and XI (b). The Table lists the velocity fields at 90 km for different horizontal phase velocities. This is necessary since we did not know the observed values for the horizontal phase velocities which must hence be treated as a variable parameter. These are two particular and relatively prominent Fourier components.

The results for June 29, 1984 at periods of 70 & 19.1 min. are given in Table XI (c) and XI (d). The velocity fields as computed from (16), (9) and (2) at 90 km are listed. To construct the actual non-monochromatic velocity profile, we need to repeat the process for every period (including those that do not have a power peak). The present results appear to be

rather low, but this is expected since we have only computed two particular Fourier components for each day.

In addition to all the above problems, we have used a model (Hatfield et al (1981)) which contains only the dynamics for our present analysis and have not used either chemistry or the background winds. Whilst recently Schubert & Walterscheid (1986) have included more chemistry, their dynamics is based on simple perturbation with a Hines gravity model and no wind effects at all. So to accomplish the task properly, we need to include not only all the chemistry, but also the proper non-perturbative dynamics with the inclusion of background winds. This is in fact one of the tasks we will be working on for our next project.

(IV) A Preliminary Study on the Behavior of Short Period Gravity Waves

(1) Preliminary Discussion

Whilst a large body of literature exists on the guidance of gravity waves, the guidance mechanisms for the internal (rather than surface) gravity waves have been principally attributed to either the structural guidance produced by unevenness in the background atmosphere, or the unevenness in the background wind profile, (Hines & Reddy [1967], Reddy, [1969]), or the "dissipative" guidance produced by unevenness in the background dissipation (Tuan [1976], Richmond [1978], Yu, et al. [1980] Tuan and Tadic [1982]). The last guidance mechanism has been specifically investigated by Richmond (1978) in a three-layer model.

In the present report we wish to focus on a particular guidance mechanism which can exist only for short-period gravity waves with periods in the range of the Brunt period (about 5 to 15 minutes), and which, so far as we are aware, has not been systematically investigated. The basic idea of the mechanism is that the Brunt period (the period for natural atmospheric oscillation) increases almost monotonically with height above 105 km (Fig. 13). A gravity wave with frequency ω from low altitude will eventually reach an altitude $z_o = z_o(\omega_b)$ where $\omega = \omega_b$. Since for $z > z_o$, $\omega > \omega_b$ gravity-wave propagation becomes impossible, the wave energy will be fully reflected earthward to produce together with reflections from the ground boundary a series of fully guided modes. Since most low altitude gravity waves have horizontal phase velocity v_{phx} less than the local speed of sound, c (Battaner & Molina [1980]), vertical propagation in the acoustic mode for $z > z_o$ is ruled out by the Hines' dispersion relation for $v_{phx} < c$.

As a preliminary investigation to illustrate the feasibility of this particular mechanism we shall consider a simple two-layer model (Wang & Tuan (1985)) with a rigid surface ground boundary (Fig. 13). The simultaneous presence of other guidance mechanisms such as the wind profile, the dissipation, or the use of a more realistic atmosphere will be postponed for a full length paper. The present preliminary treatment is intended to explore only the basic idea of this ducting mechanism.

In view of the fact that the guidance mechanism under discussion is always in effect whereas some of the other guidance mechanisms, such as the

wind profile, may not always be in effect (the wind may, for instance, be perpendicular or at a large angle to the direction of wave propagation), one would expect that in general simultaneous observations of fluctuations below and above the Brunt period curve (Fig. 13) (e.g. the simultaneous observations of the OH or 5577 OI and the 6300Å red line or the P.R.D. radar, etc.) should reveal that short-period fluctuations in the lower region would tend to occur more frequently than the upper region. This guidance mechanism may then be considered as a filter which filters out the low altitude short-period gravity wave components, leaving only the longer period components to penetrate to higher altitudes.

If a more detailed calculation using a more realistic atmosphere should show that the suggested filtering process is significant, then simultaneous experimental observations above and below the Brunt frequency curve may verify this process. We may add that short period oscillations can still occur at high altitudes (owing, for instance, to high altitude sources or to Doppler-shift of longer-period waves by winds, etc.) The removal of these short-period oscillations at say the 6300Å peak by high altitude dissipation, either through viscosity or heat conduction, is unimportant, since at that altitude, the dissipation is either insignificant (for $v_{phx} > 120$ m sec^{-1}), or the wave amplitude is already too small (because of ducting) to be of interest.

2. Method

We approximate the variation of the Brunt period in Fig. 13 by two layers. The atmosphere is assumed to be uniform and isothermal in each

layer. The atmospheric parameters for each layer are taken to be the same as those adopted by Thome (1968), although we differ from Thome by adding a rigid surface ground boundary. The Brunt periods for these two layers are T_{bI} = 5.4 min for the lower layer and T_{bII} = 14.8 min for the top layer. The advantage for such a model is that analytic solutions are possible and that a Hines' dispersion relation can be written down for each layer. Thus,

$$k_I^2 = \frac{\omega_{bI}^2 - \omega^2}{v_{phx}^2} - \frac{\omega_{aI}^2 - \omega^2}{c_I^2} \tag{19}$$

$$k_{II}^2 = \frac{\omega_{bII}^2 - \omega^2}{v_{phx}^2} - \frac{\omega_{aII}^2 - \omega^2}{c_{II}^2} \tag{20}$$

where v_{phx} is the horizontal phase velocity and ω_a the acoustic cut-off frequency.

Quite obviously, if $T_{bI} < T < T_{bII}$ (such as the eight minute period wave in Fig. 13) and $v_{phx} < c$,

$$k_I^2 > 0, \; k_{II}^2 = (i\kappa)^2 < 0 \tag{21}$$

For the 8 min. wave, k_I is a real vertical propagator whilst k_{II} is pure imaginary. Within each isothermal layer, the hydrodynamic equations can be quickly reduced to single second-order equations. The equations for the pressure variation (normalized to constant amplitude) are given by:

$$\left(\frac{d^2}{dz^2} + k_I^2 \right) \psi_I = 0 \quad (0<z<z_o) \tag{22}$$

$$\left(\frac{d^2}{dz^2} + k_{II}^2 \right) \psi_{II} = 0 \quad (z>z_0) \tag{23}$$

where $\psi = \omega\Delta p/\rho_o^{1/2} \alpha \Delta p$, the actual pressure variation,

z_o = height level which separates II from I

The solutions can be easily obtained with the following rigid surface condition at z = 0, the finite energy requirement at $z\to\infty$, plus the interfacial boundary condition at $z = z_o$;

$$\frac{\partial \psi_I}{\partial z}\bigg|_{z=0^-} - \bar{\eta}_I \psi_I\bigg|_{z=0} = 0 \tag{24}$$

$$\psi_{II} \underset{z\to\infty}{\to} e^{-\kappa z} \quad (\kappa>0 \text{ and real}) \tag{25}$$

$$\frac{Dp_I}{Dt}\bigg|_{z=z_o} = \frac{Dp_{II}}{Dt}\bigg|_{z=z_o} \tag{26}$$

$$\Delta w_I\bigg|_{z=z_o} = \Delta w_{II}\bigg|_{z=z_o} \tag{27}$$

where $\bar{\eta}_I = \left[\frac{1}{2} \frac{\gamma g}{c_1^2} - \frac{g}{c_1^2} \right]$ and equation (24) is the rigid surface condition for ψ corresponding to the vertical velocity $\Delta w_I(z=0) = 0$.

Applying (24) and (25) to solutions of (22) and (23), we obtain

$$\psi_I = A \left[e^{-ik_I z} + \frac{k_I - i\bar{\eta}_I(0)}{k_I + i\bar{\eta}_I(0)} e^{ik_I z} \right] \tag{28}$$

$$\psi_{II} = C e^{-\kappa z} \tag{29}$$

Applying the interfacial boundary conditions (26) and (27) we obtain the following general dispersion relation for two uniform isothermal layers plus a rigid ground boundary:

$$\frac{1}{\rho_{oI}(z_o)} \frac{[k_I^2 + \bar{\eta}_I^2]}{\left[k_I^2 + \bar{\eta}_I^2 - \frac{(\omega_{bI}^2 - \omega^2)}{g} \bar{\eta}_I \right] - \frac{(\omega_{bI}^2 - \omega^2)}{g} k_I \cot(k_I z_o)}$$

$$= \frac{1}{\rho_{oII}(z_o)} \frac{[\kappa + \bar{\eta}_{II}(z_o)]}{[\kappa + \bar{\eta}_{II}(z_o) - \frac{(\omega_{bII}^2 - \omega^2)}{g}]} \tag{30}$$

By substituting (19) and (20) into (30) we can eliminate k_I and $k_{II} = i\kappa$ to obtain a single transcendental equation in v_{phx} which can be readily seen to contain an infinite but discrete number of solutions for each ω, or wave period. Fig. 14 shows a plot of some of the lower discrete states corresponding to numerical solutions to the equation for v_{phx} for wave periods 5.5, 6, 7, 8, 9, 10, 11, 12, 13 and 14 minutes. As can be seen from Fig. 14, for sufficiently low horizontal phase velocities, the

discrete modes are so close to each other that they form essentially a continuum for practical purposes.

3. Remarks & Comments

When a more realistic COSPAR atmospheric model is used, our ongoing investigation (Wang and Tuan (1985)) would seem to show that whilst there are important quantitative differences, there is little difference in the basic physics of the guidance mechanisms. The results for the first few guided modes show considerable resemblance to the two-layer model (Fig. 14) but the locations of the modes are different.

From Fig. 13, the Brunt period curve shows a height level of slightly below 200 km at a period of 9 min. The COSPAR-based calculation shows that for horizontal phase velocities ranging from 96 to 244 m sec^{-1}, the low altitude (<100 km) waves with less than 9 min period become evanescent when they reach 200 km or less and become negligible above 220 km. Using airglow as an example, the 6300Å luminosity profile peaks at 260-290 km and cuts off fairly sharply below the peak to about 220 km and is negligible below. Since the dissipation does not become important until 250 to 300 km, where the wave has long since been filtered out, the suggested guidance mechanism does appear to be significant in removing the short-period components from the 6300Å red line for low-altitude sources. In general there are far more low-altitude sources than high-altitude (above 100 km) sources and the latter usually generate the large-scale T.I.D.'s which can

on occasion be identified from their high horizontal phase velocities (~400-700 m sec^{-1}).

Large amplitude waves can produce short-period oscillations associated with the local Brunt period (Tuan et al [1979]). But these oscillations vary with height ranging from 5 min. at mesospheric heights to 12 min. at ionospheric altitudes and will not contribute to the short-period (<10 min) behavior in the upper region.

The presence of horizontal winds can alter the horizontal phase velocities of the guided modes just as it does for the long-period guided modes (Reddy, [1969]). However, the probability that it can have a component (parallel to the wave propagation) large enough to Doppler shift a 9 min. period to less than 5 min. at ionospheric height levels can be estimated to be less than 35%.

In recent times there have been considerable interest in short period fluctuations which may be detected through many different techniques including mesospheric airglow observation (e.g. Myrabo et al [1983], Peterson [1979], Peterson [1985], Clairemidi et al [1985]), or the P.R.D. radar system, (e.g. Manson & Meek [1980], or Manson al [1981]) etc). These short-period fluctuations are often of the order of minutes or low tens of minutes, well within the range of the Brunt-period curve (Fig. 13). The radar system can be extended to accommodate the height range below and above most parts of the Brunt-period curve. In the case of airglow, since the mesospheric emissions are for the most part located below the

Brunt-period curve, simultaneous observations with the 6300Å OI can readily cover the range. The simultaneous observations will have to be made at less than 1 minute intervals. One may then expect from these discussions that on an average the frequency of occurrence of short-period fluctuations in the higher altitude region (above the Brunt-period curve) should be less than the lower region.

Bibliography

1. Battaner E. and A. Molina, J. Geophys. Res. 85, 6803, (1980).

2. Beamish, N.M., M. Sc. Thesis, University of Manchester (1977).

3. Beamish, N.M. and M.B. Priestley, Appl. Statist., 30, 41, (1981).

4. Chiu, Y.T. and B.K. Ching, Geophys. Res. Lett. 5, 539 (1978).

5. Chairmidi, J., M. Herse and G. Moreels, Planet. Space Sci. 33, 1013, (1985).

6. Dudis, J.J. and C.A. Reber, Geophys. Res. Lett., 3, 9727, (1976).

7. Feigenbaum, M.J., Physics 7D, 16, (1983).

8. Gasser, T., Research Report no. 4, Fachgrippe fur Statistik, Eidgencessiche Technische, Hochschule, Zurich (1974).

9. Hatfield, R., T.F. Tuan, and S.M. Silverman, J. Geophysics Res. 86, 2429, (1981).

10. Hines, C.O., and C.A. Reddy, J. Geophysics, Res. 72, 1015, (1967).

11. Hines, C.O. and C.A. Reddy, J. Geophys. Res. 90, 7995, (1985).

12. Manson, A.H. and C.E. Meek, J. Atmos. Term. Phys. 42, 103, (1980).

13. Manson, A.H., C.E. Meek and J.B. Gregory, J. Atmos. Terr. Phys. 43, 35, (1981).

14. Martin, R.D., Proc. International Time Series Meeting, University of Nottingham, England, North Holland, Amsterdam (1979).

15. Myrabo, H.H., C.S. Deehr, and G.G. Sivjee, J. Geophys. Res., 88, 9255-9259, (1983).

16. Peterson, A.W., Appl. Opt. 18, 3390, (1979).

17. Peterson, A.W., Private Communication (1985).

18. Porter, H.S. and T.F. Tuan, J. Atmos. Terr. Phys. 36, 135, (1974).

19. Reddy, C.A., Tech. Note IN-43, Nat. Counc. Atmos. Res., Boulder, Colorado, (1969).

20. Richmond, A.D., J. Geophys. Res., 83, 1385, (1978).

21. Schoeberl, M.R., D.F. Strobel and J.P. Apouzee, J. Geophys. Res., 88, 5249, (1983).

22. Schubert, G. and R.L. Walterscheid, Trans. Amer. Geophys. Union, 66, 97, (1985).

23. Testud, J. and P. Francois, J. Atmos. Terr. Phys. 33, 765, (1971).

24. Thome, G.D., J. Geophys. Res. 73, 6319, (1968).

25. Tuan, T.F., R. Hedinger, S.M. Silverman, and M. Okuda, J. Geophys. Res. 84, 393, (1979).

26. Tuan, T.F. and D. Tadic, J. Geophys. Res. 87, 1648, (1982).

27. Ulrych, T.J., J. Geophys. Rec. 77, 1396, (1972).

28. Ulrych, T.J., D.E. Smylie, O.G. Jensen and G.B.C. Clark, J.Geophys. Res. 78, 4959, (1973).

29. Ulrych, T.J. and T.N. Bishop, Rev. Geophys. and Space Phys. 13, 183, (1975).

30. Wahba, G., Tech. Report no. 536, Dept. of Statistics, University of Wisconsin, (1968).

31. Wang, D.Y. and T.F. Tuan, Trans. Amer. Geophys. Union, 66, 997, (1985).

32. Yu, L., T.F. Tuan and H. Tai, J. Geophys. Res., 85, 1297, (1980).

Data
Wyoming
June 23 1984

Fig. 1a

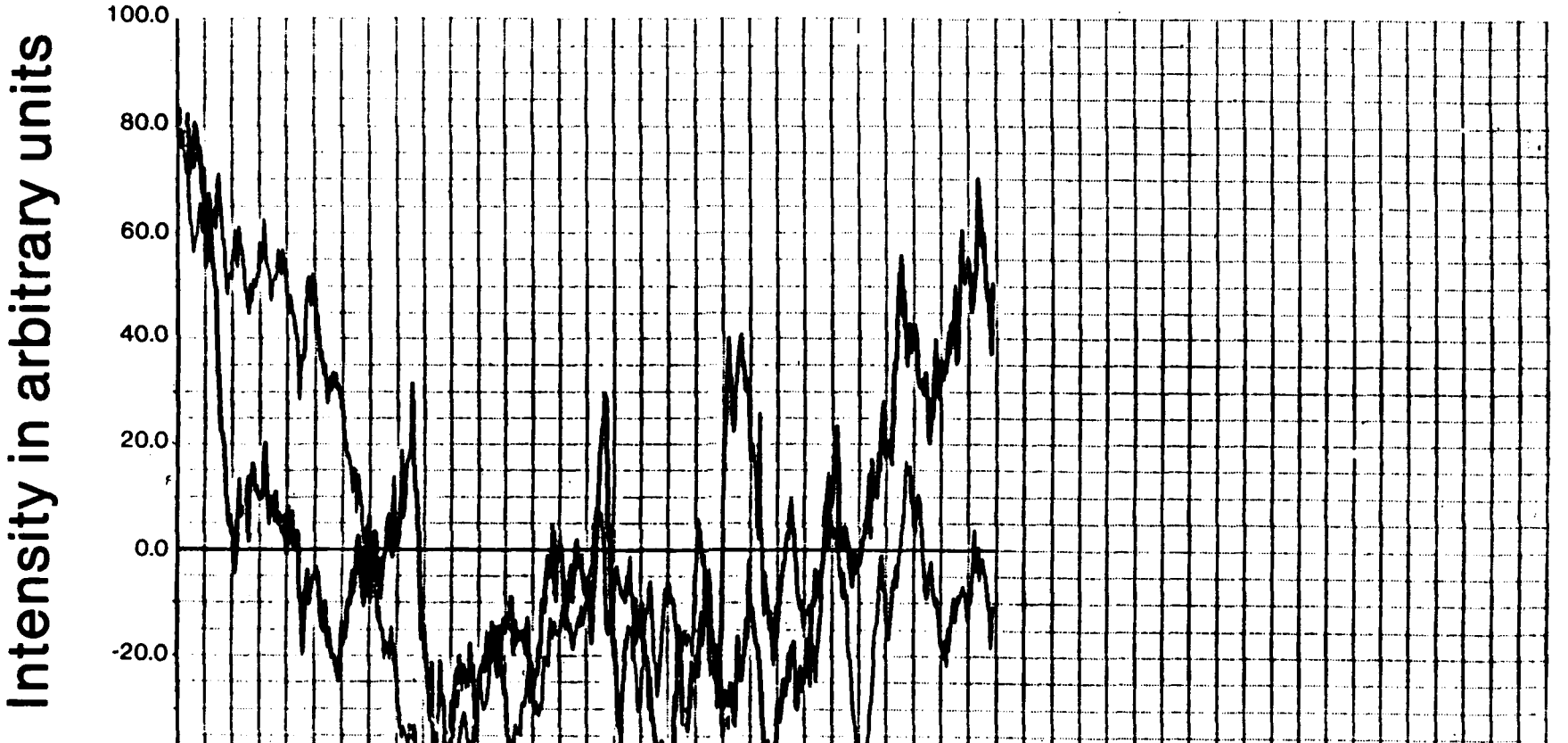

Cross Convariances
Wyoming
June 23 1984

Fig. 1b

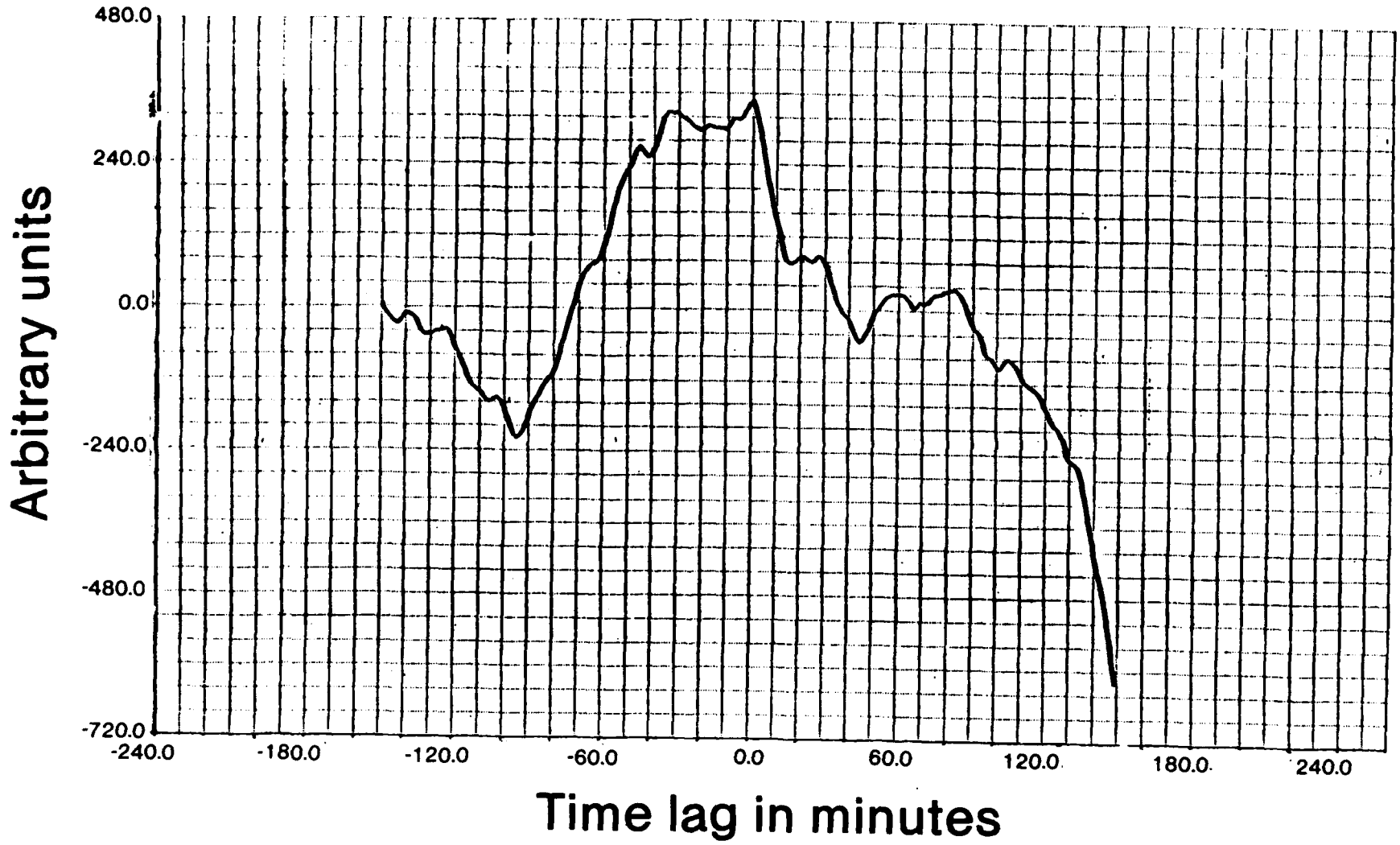

Power Spectrum
Wyoming
June 23, 1984
Cross spectrum

Fig. 1c

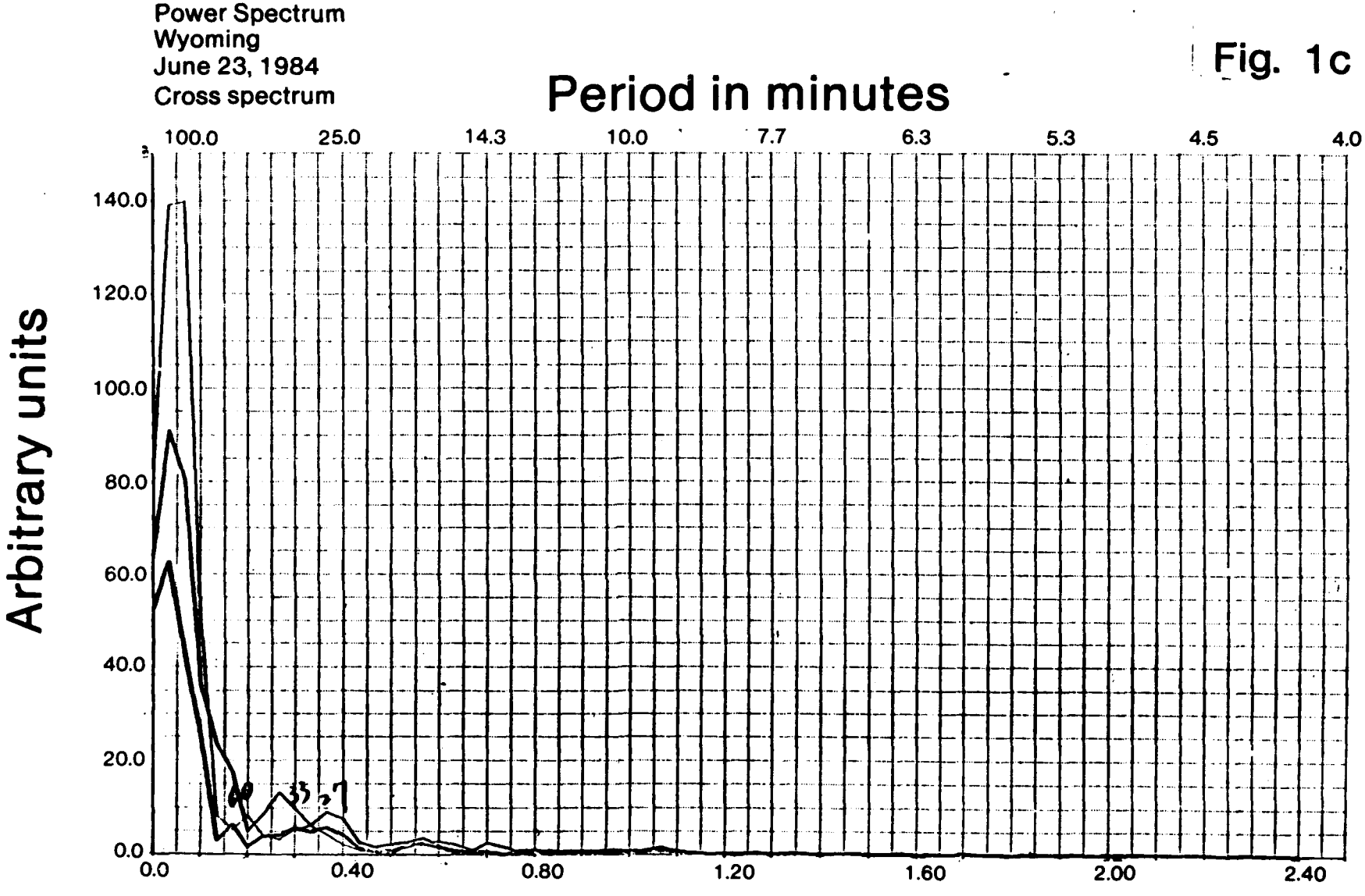

Data
Wyoming
June 27, 1984

Fig. 2a

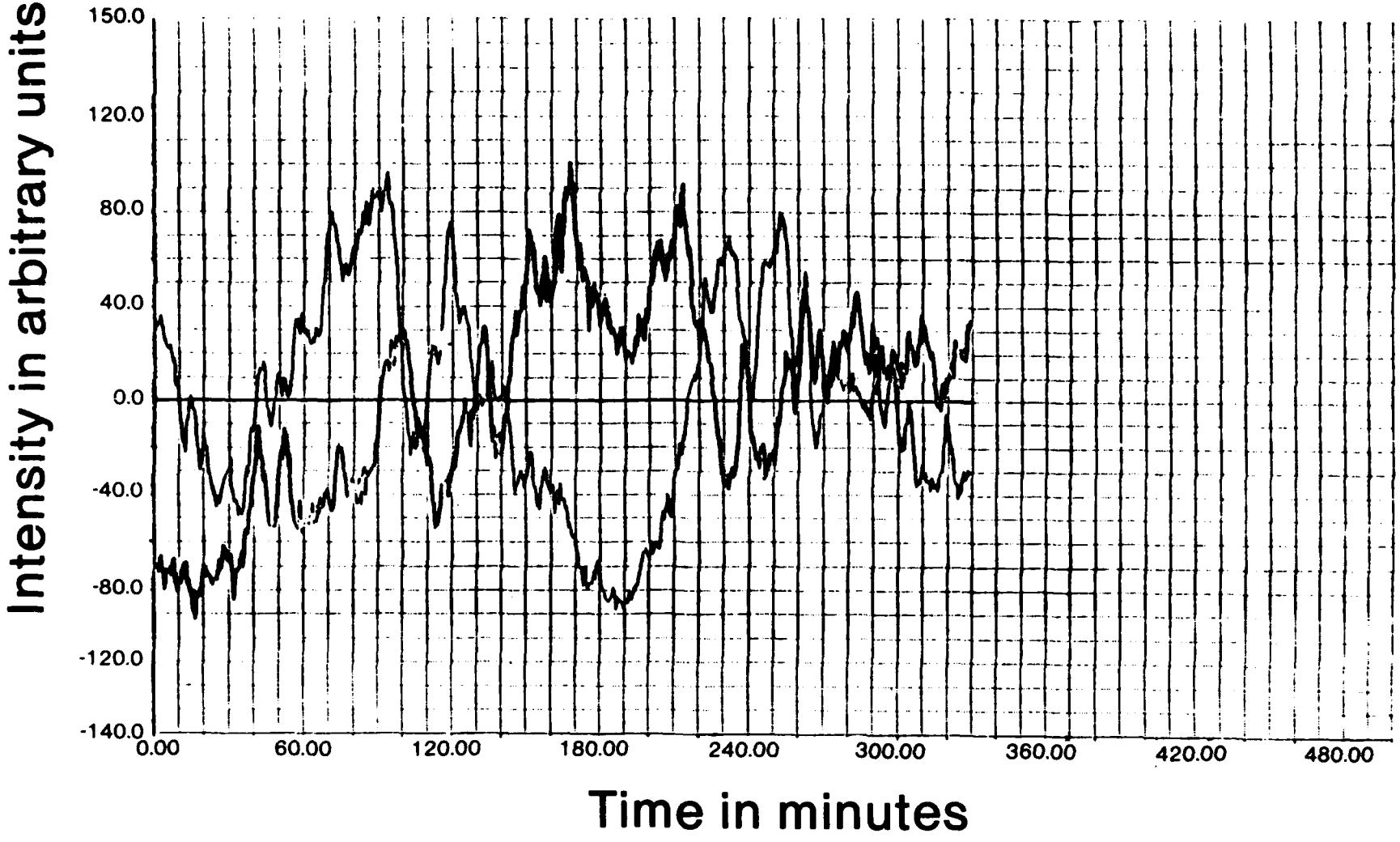

Cross convariances
Wyoming
June 27, 1984

Fig. 2b

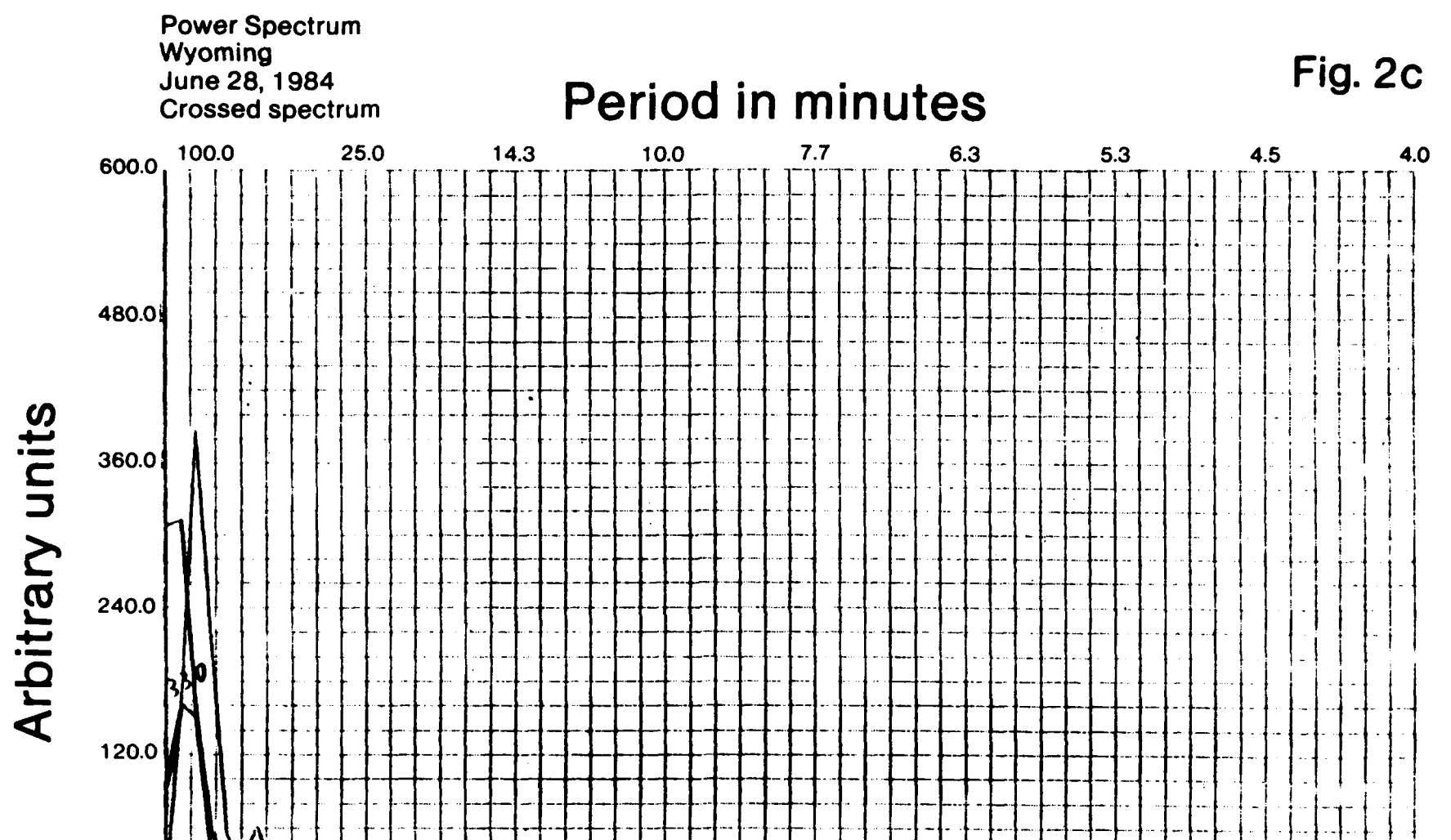
Power Spectrum
Wyoming
June 28, 1984
Crossed spectrum
Period in minutes
100.0
25.0
14.3
10.0
7.7
6.3
5.3
4.5
4.0
600.0
480.0
360.0
240.0
120.0
0.0
Arbitrary units
0.00
0.40
0.80
1.20
1.60
2.00
2.40
Frequency, min-1

Fig. 2c

Data
Wyoming
June 29, 1984

Fig. 3a

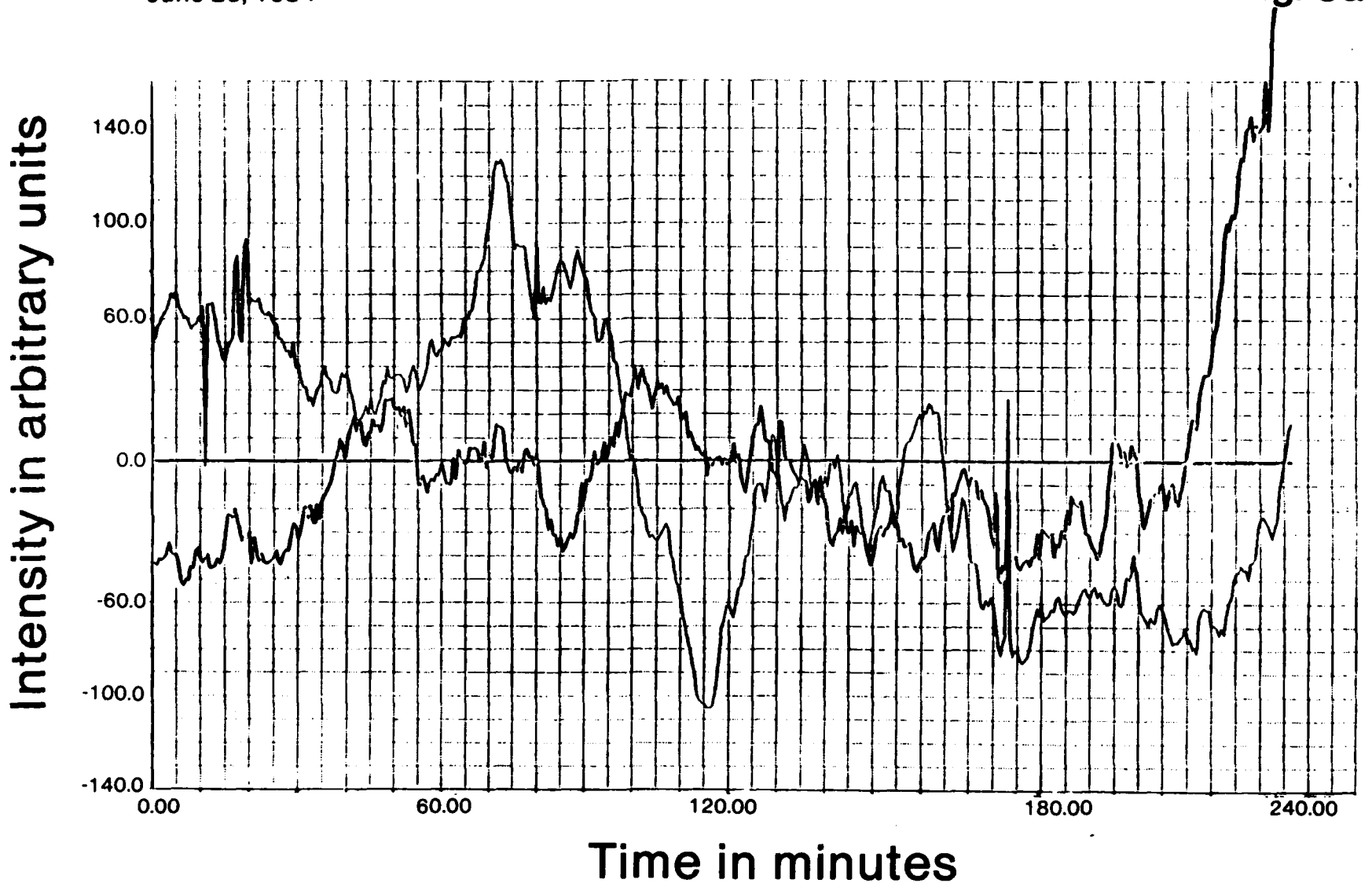

Cross Covariances
Wyoming
June 29, 1984

Fig. 3b

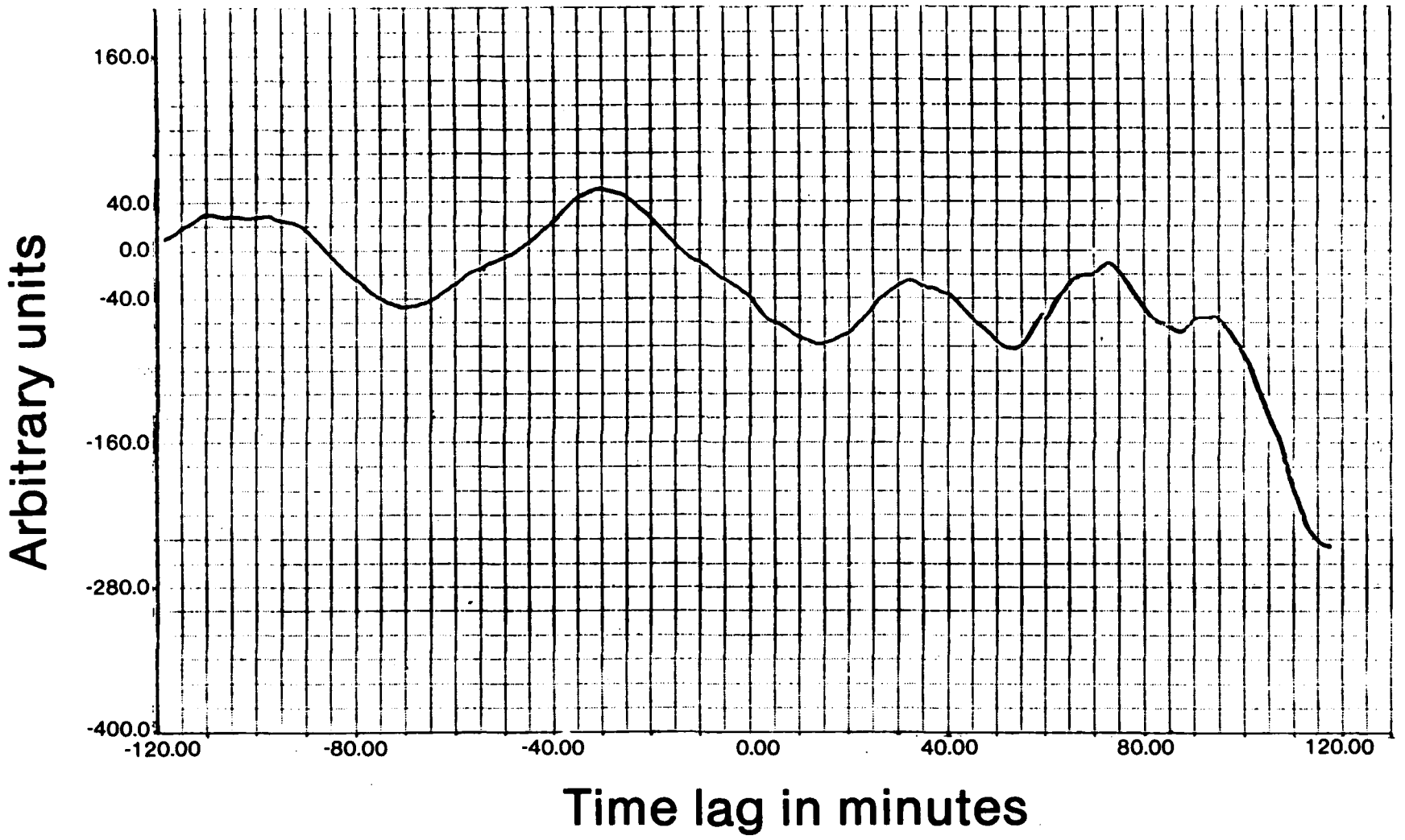

Power Spectrum
Wyoming June 29, 1984

Fig.3c

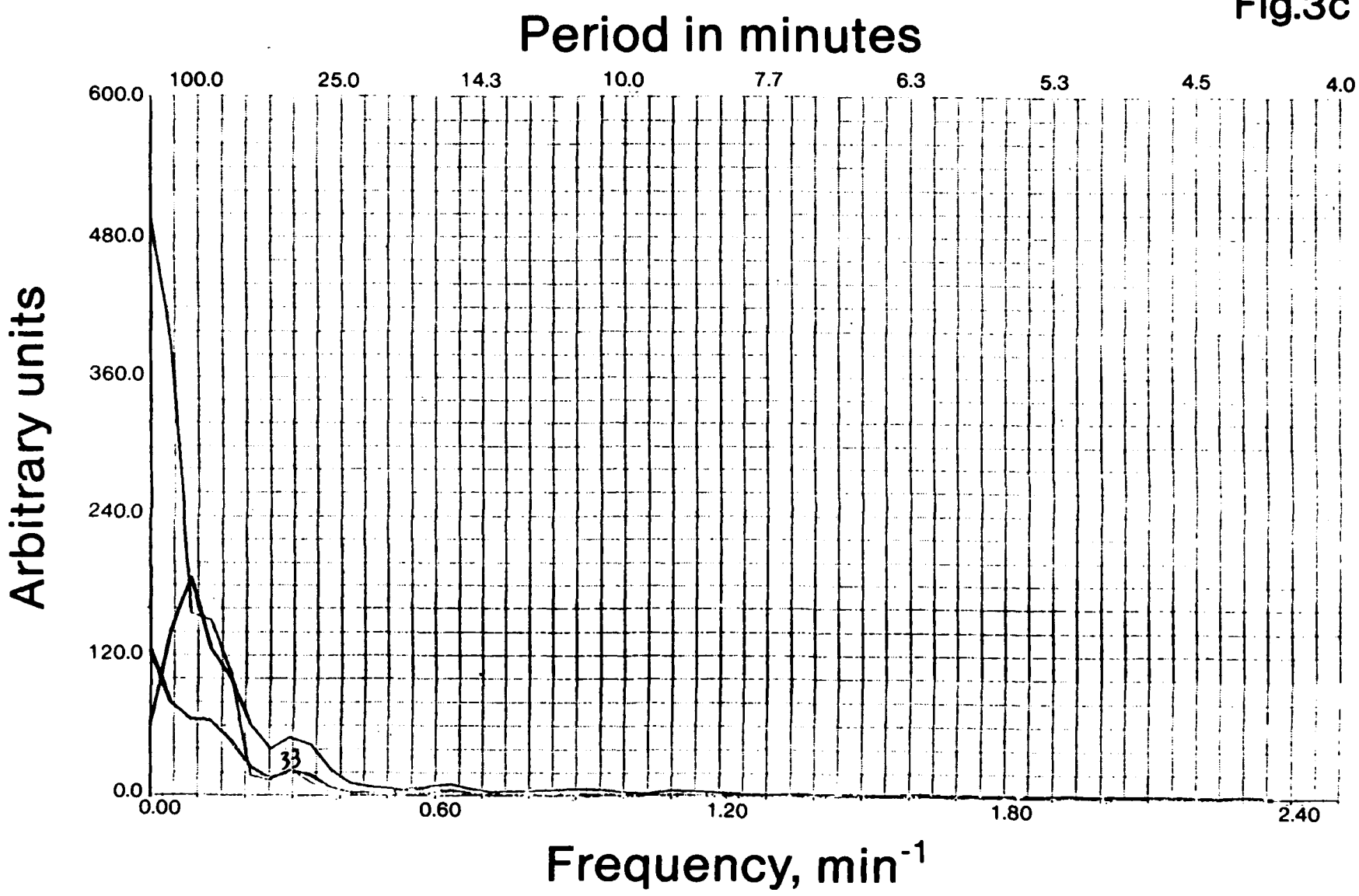

Data
Wyoming
June 23, 1984
OI 5577

Fig. 4a

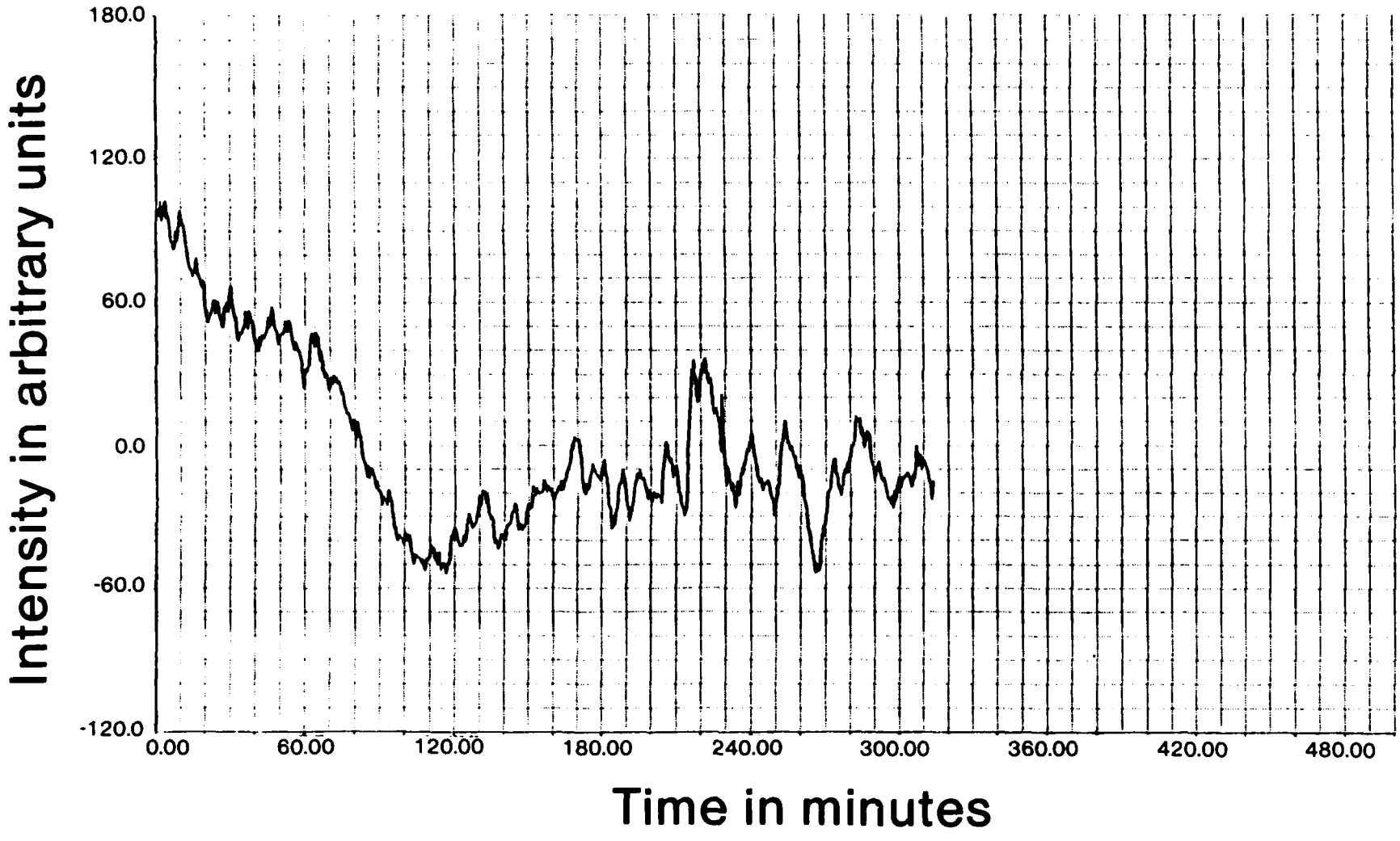

Maximum entropy method
M = 0.50 N
Noise level = 806.5018
Wyoming
June 23, 1984
OI 5577

Fig 4b

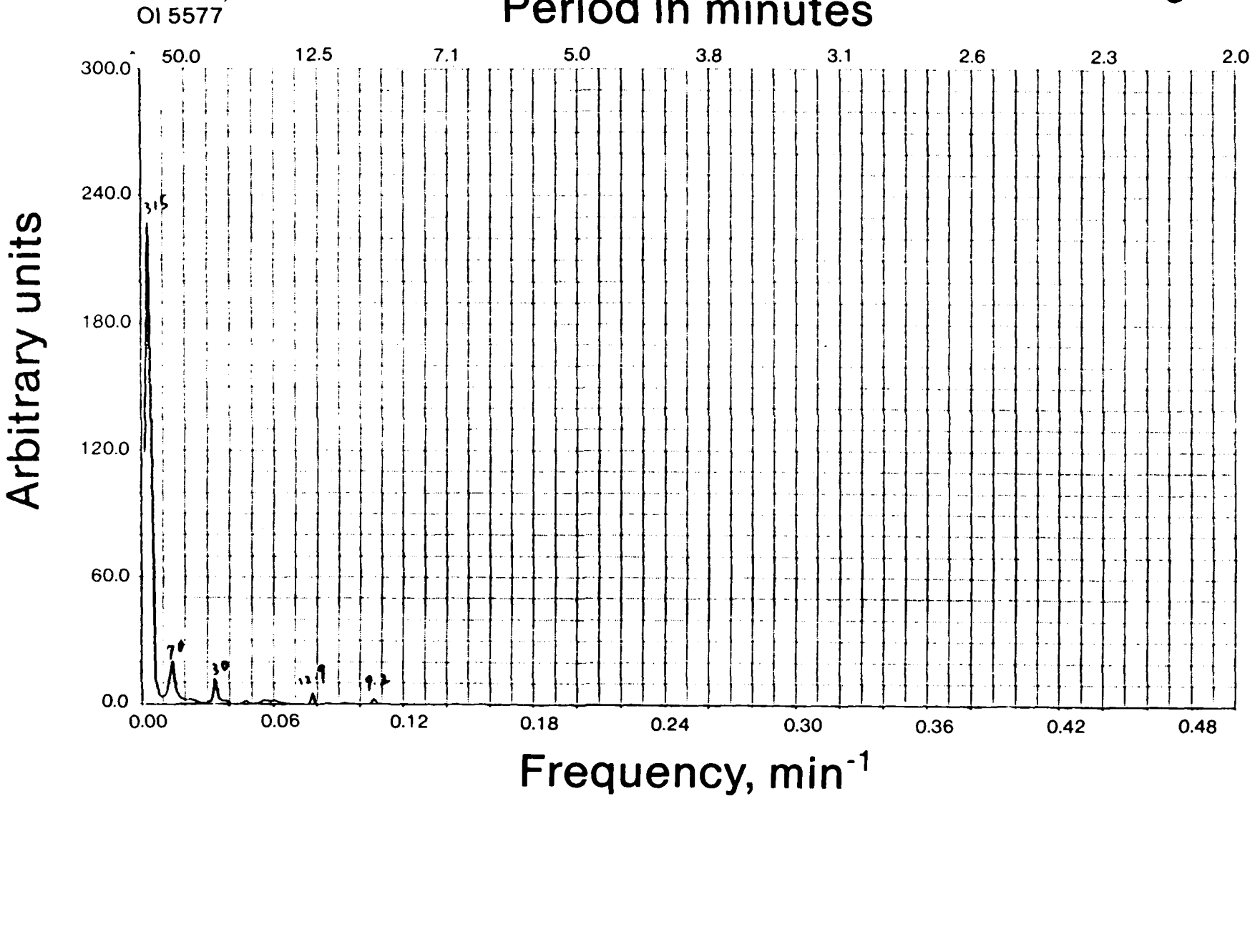

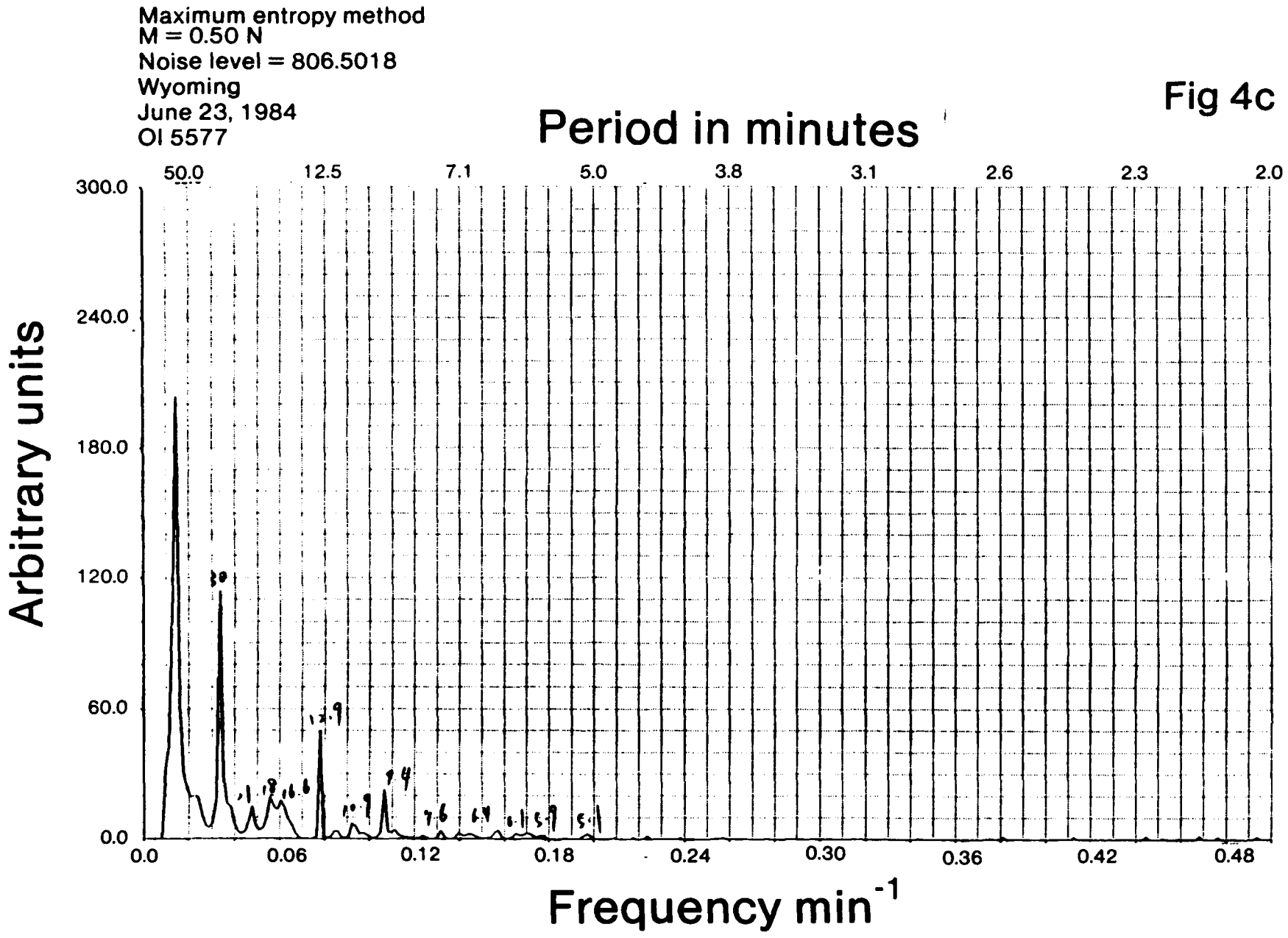
Maximum entropy method
M = 0.50 N
Noise level = 806.5018
Wyoming
June 23, 1984
OI 5577
Period in minutes
50.0
12.5
7.1
5.0
3.8
3.1
2.6
2.3
2.0
300.0
240.0
180.0
120.0
60.0
0.0
Arbitrary units
0.0
0.06
0.12
0.18
0.24
0.30
0.36
0.42
0.48
Frequency min-1

Fig 4c

Data
Wyoming
June 23, 1984
OH 7900

Fig.5a

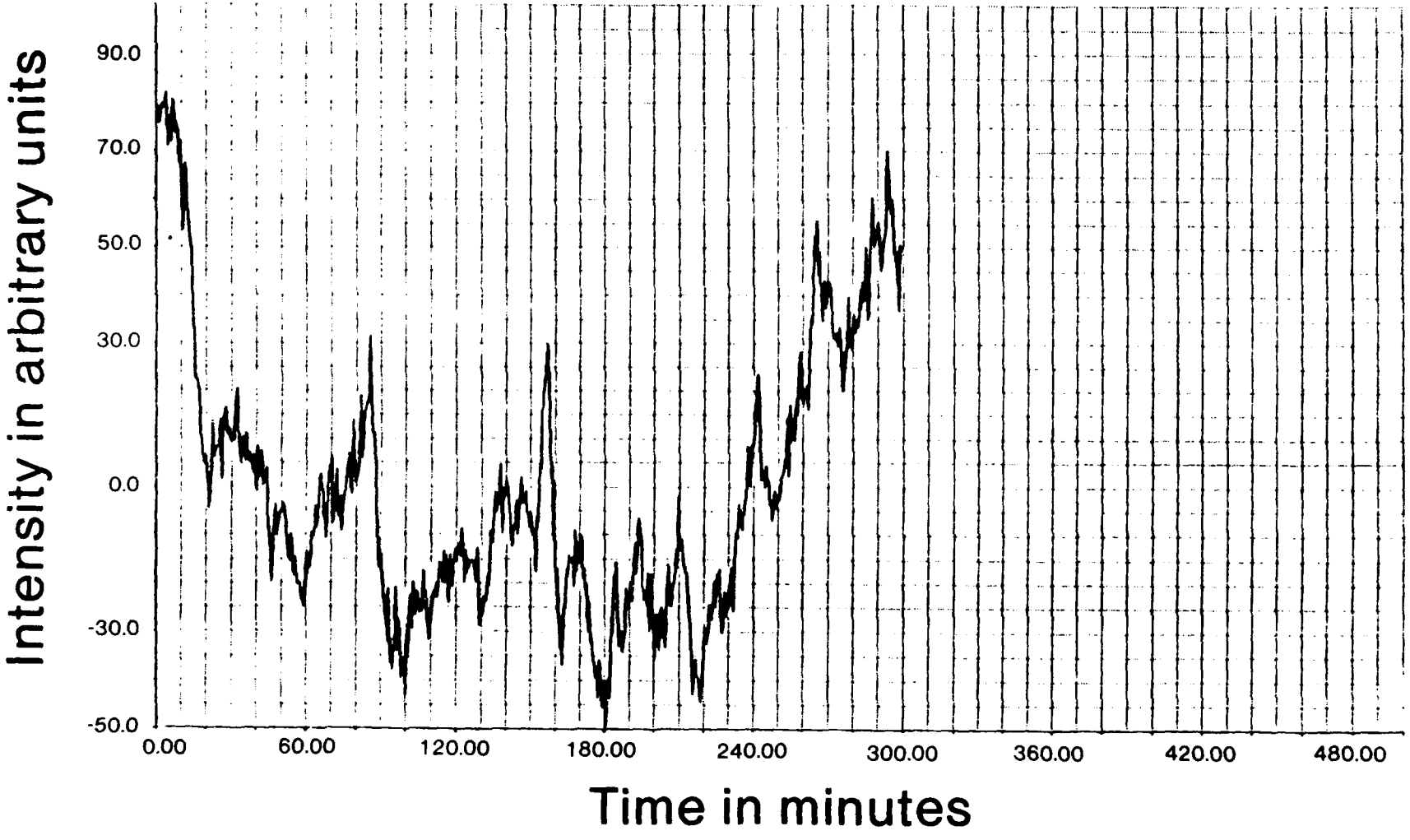

Maximum entropy method
M = 0.50 N
Noise level = 1413.3640
Wyoming
June 23, 1984
OH 7900

Fig 5b

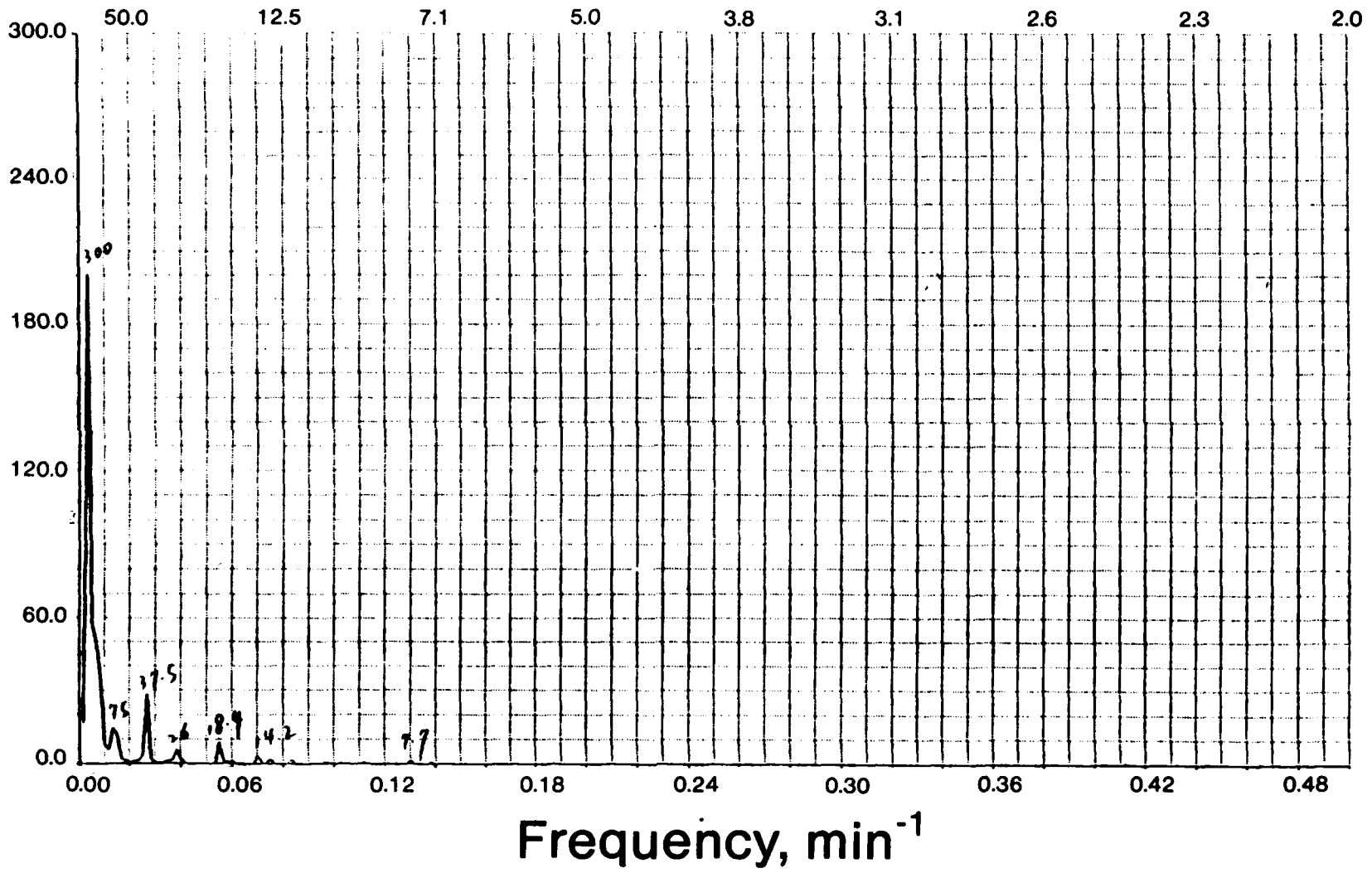

Maximum entropy method
M = 0.50 N
Noise level = 1413.3640
Wyoming
June 23, 1984
OH 7900

Fig 5c

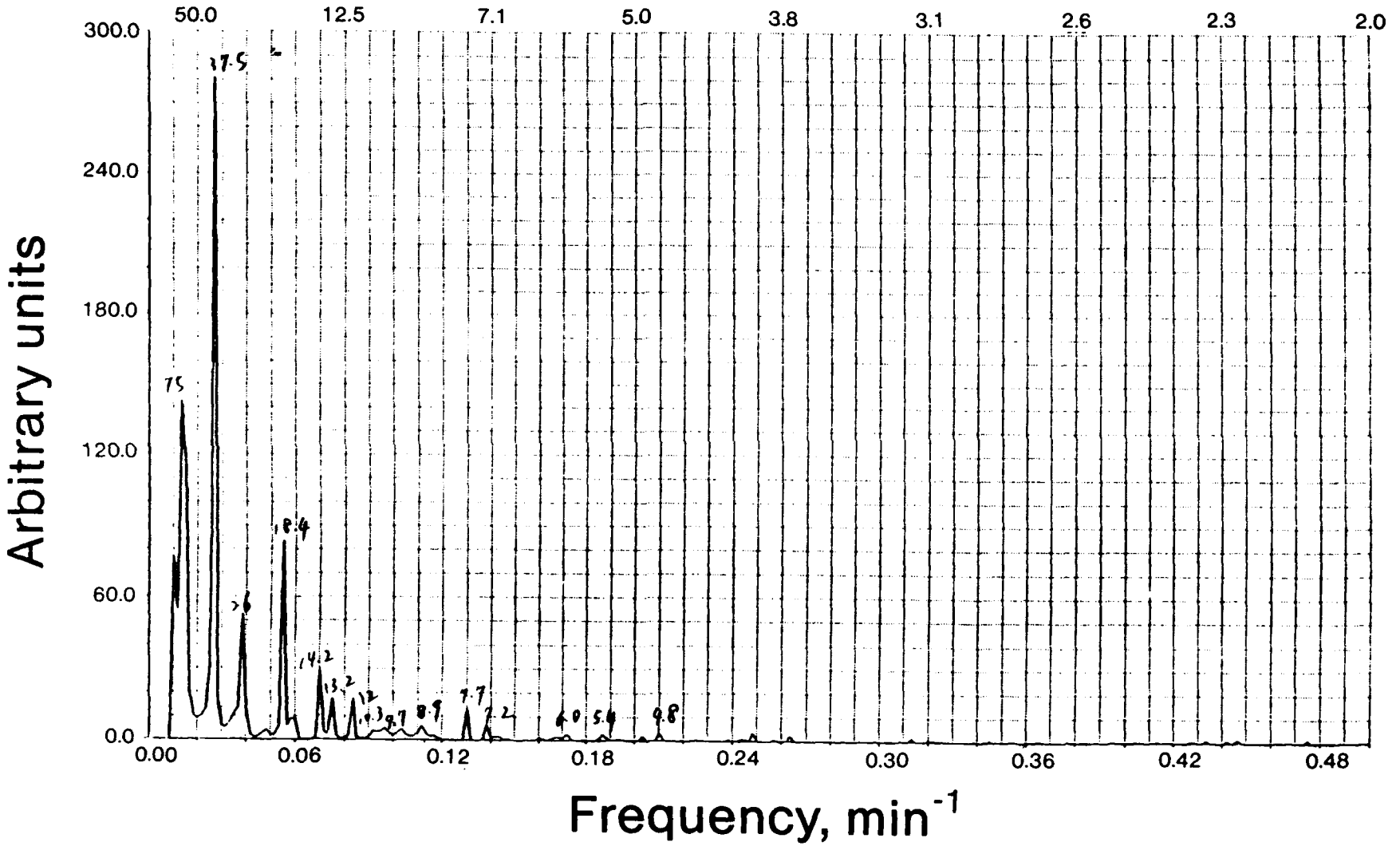

Data
Colorado
June 23, 1984
OI 5577

Fig. 6a

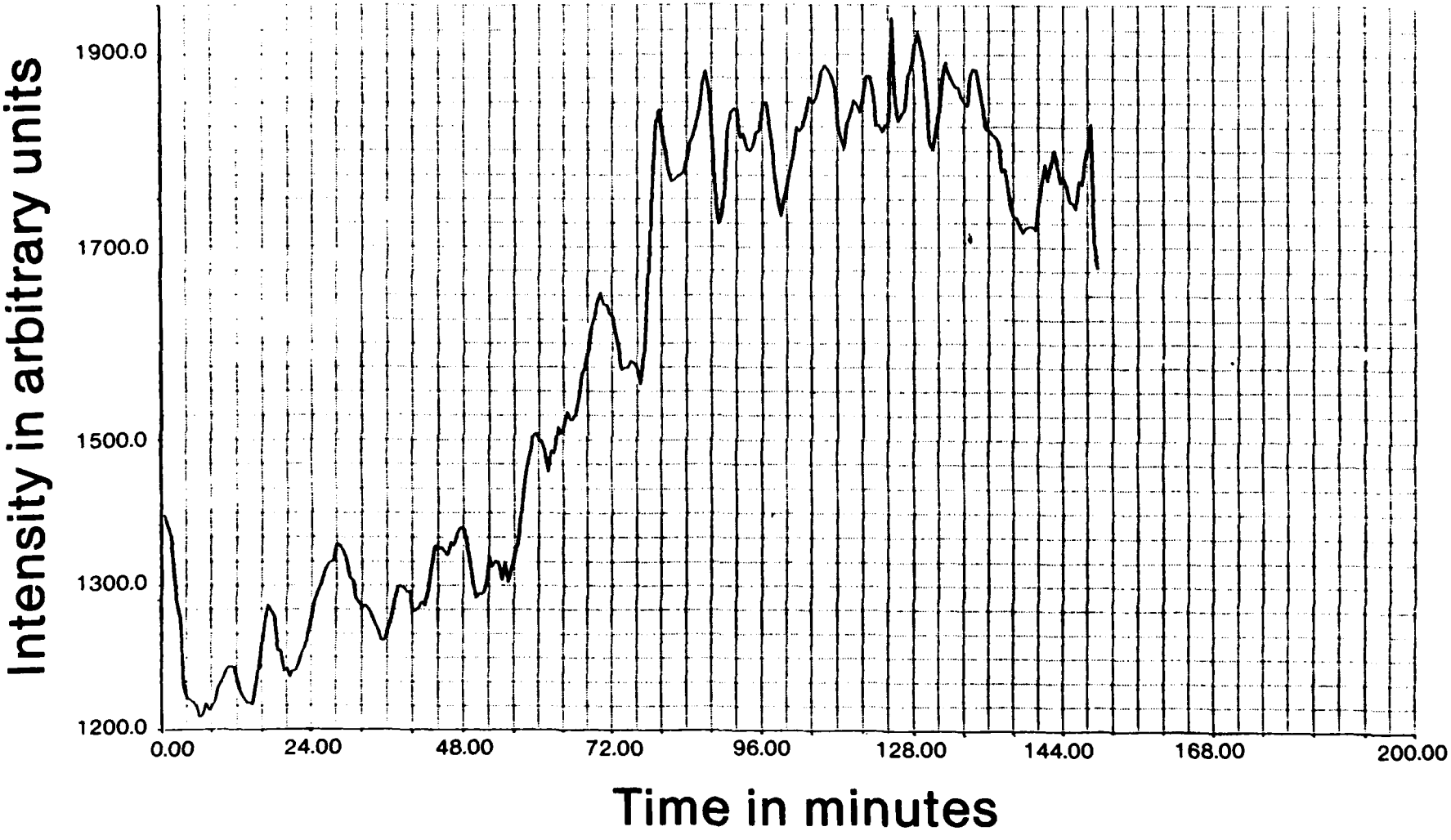

Maximum entropy method
M = 0.50 N
Noise level = 201.4970
Colorado
June 23, 1984
OI 5577

Fig 6b

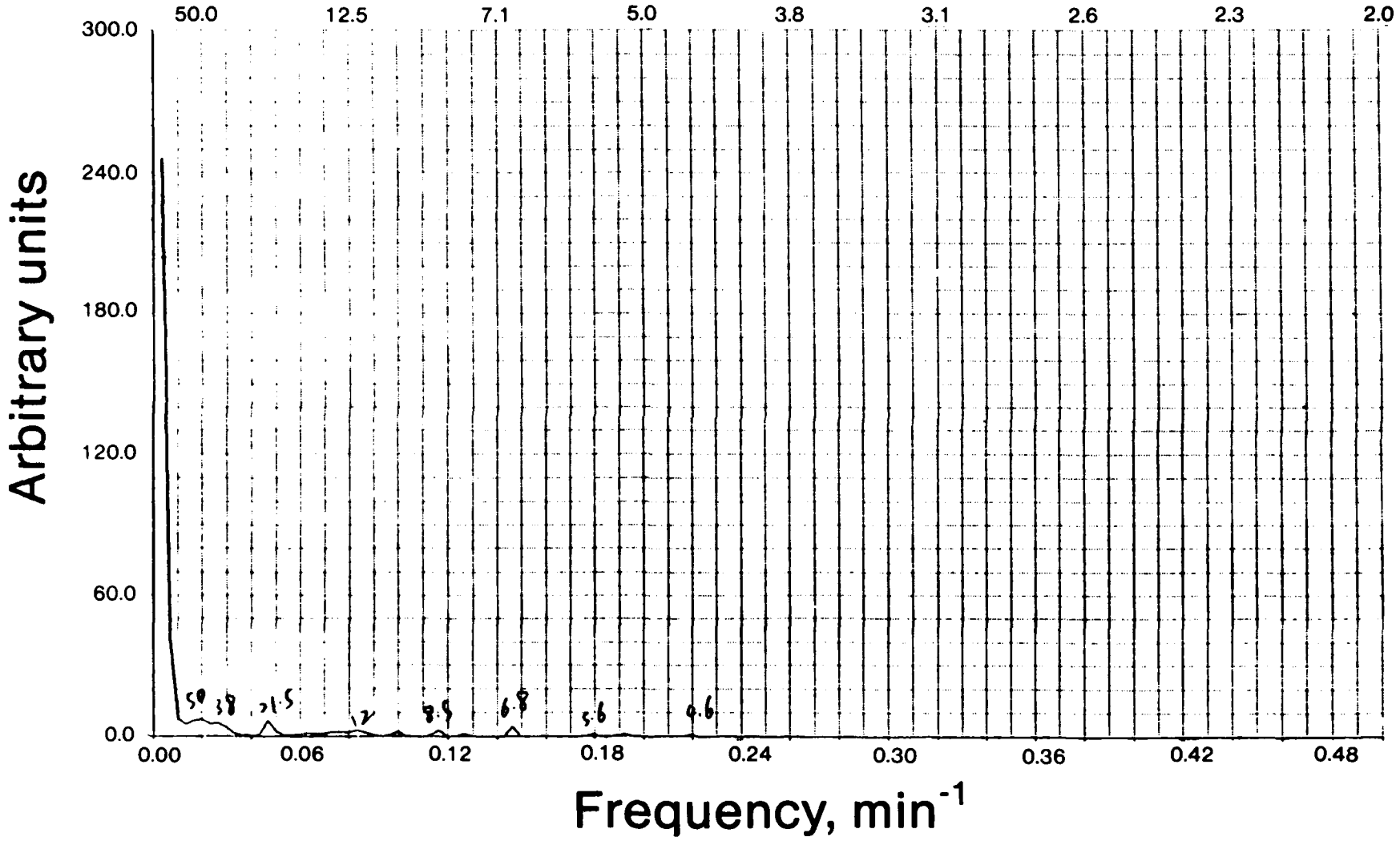

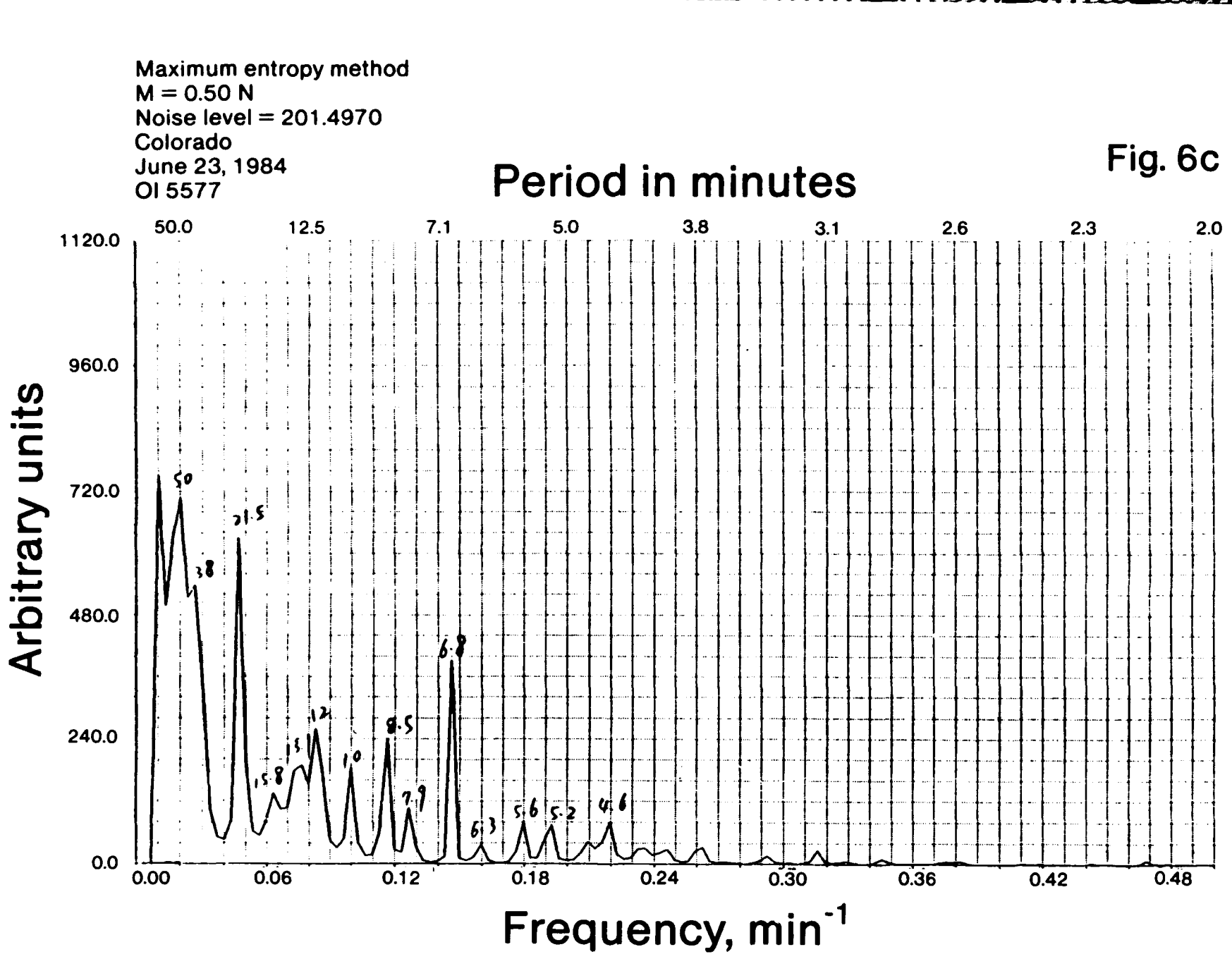
Maximum entropy method
M = 0.50 N
Noise level = 201.4970
Colorado
June 23, 1984
OI 5577
Period in minutes
50.0
12.5
7.1
5.0
3.8
3.1
2.6
2.3
2.0
1120.0
960.0
720.0
480.0
240.0
0.0
Arbitrary units
50
38
21.5
15.8
15
12
10
8.5
7.9
6.8
6.3
5.6
5.2
4.6
0.00
0.06
0.12
0.18
0.24
0.30
0.36
0.42
0.48
Frequency, min-1

Fig. 6c

Data
Colorado
June 23 1984
Radiometry

Fig. 7a

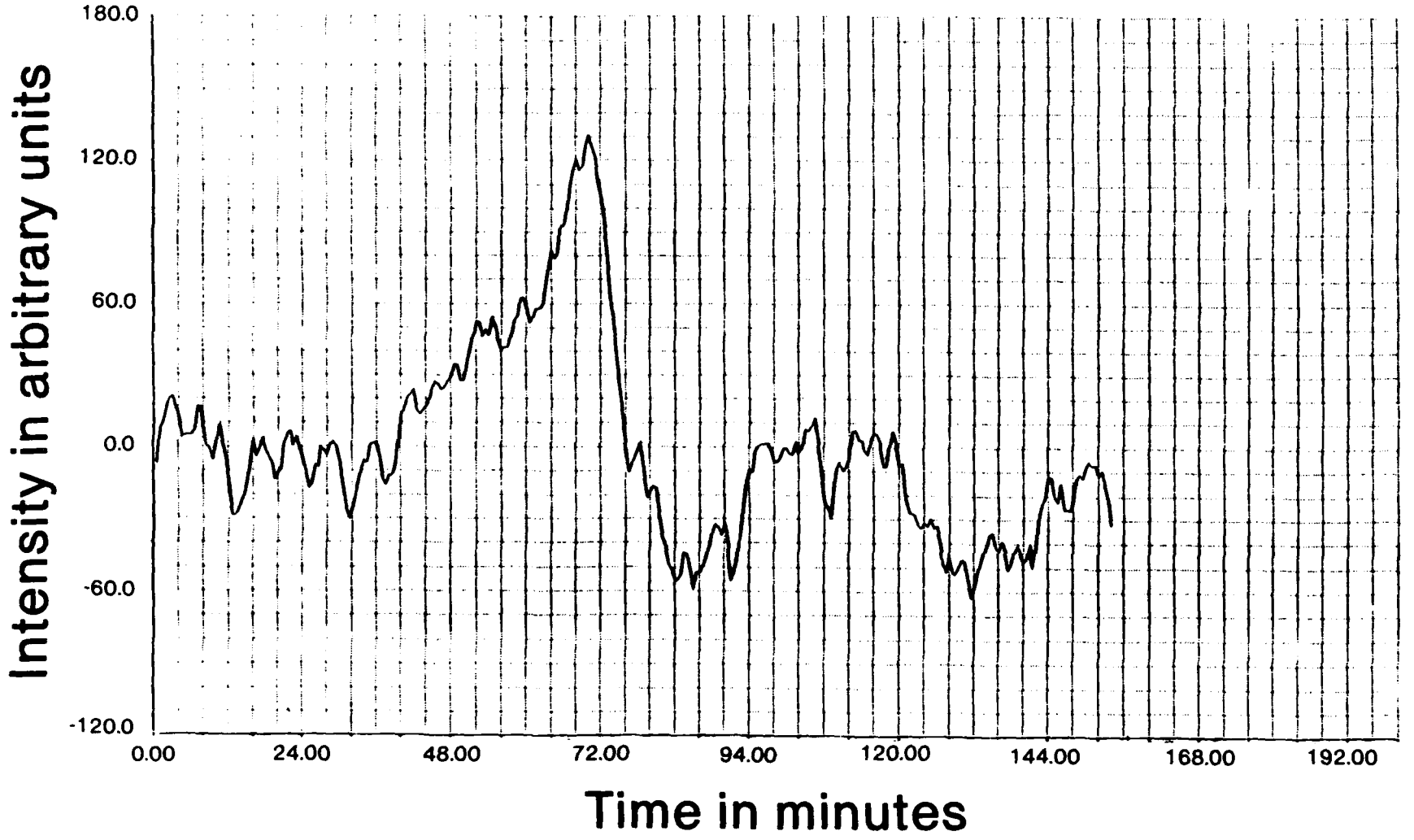

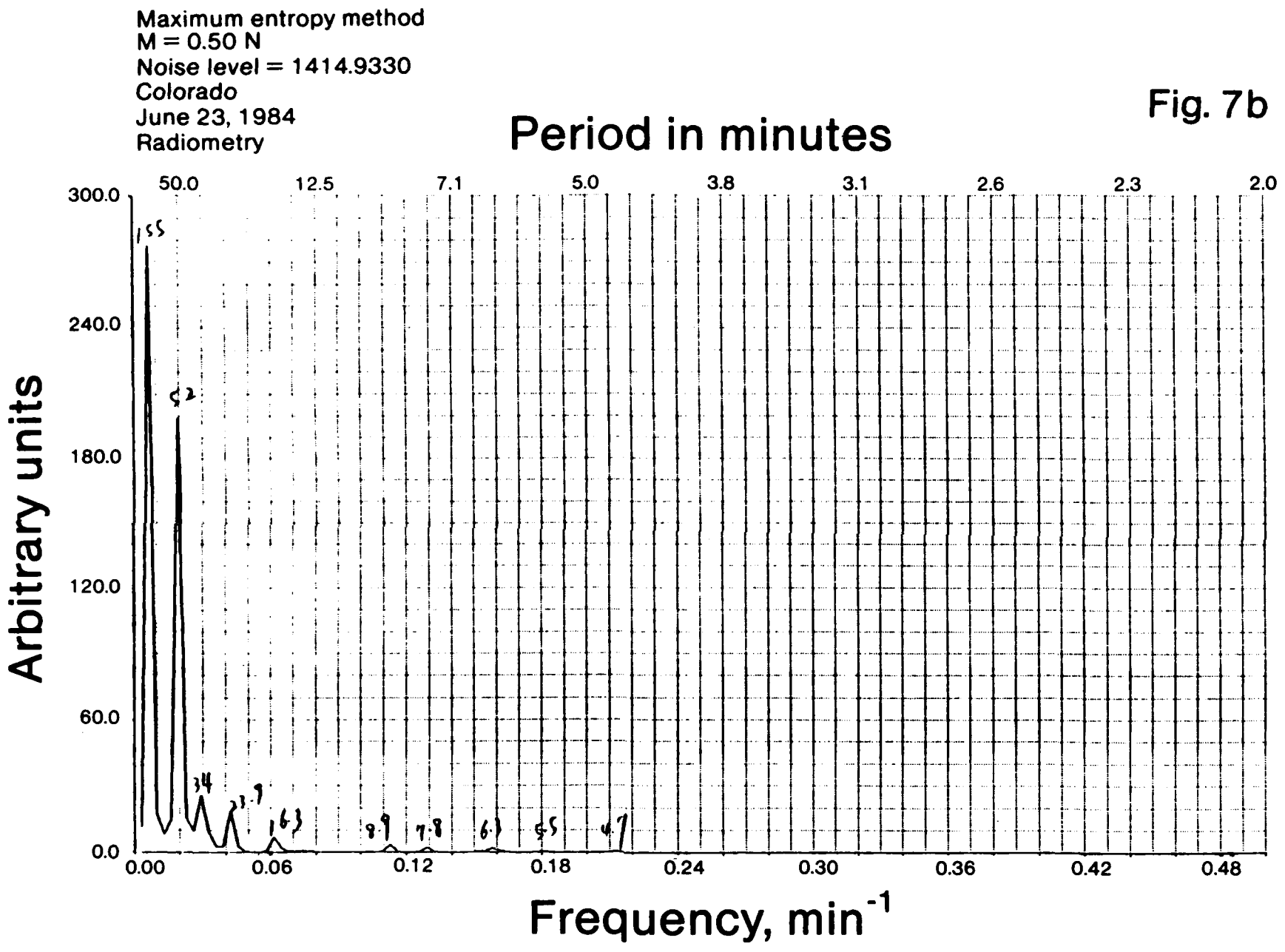
Maximum entropy method
M = 0.50 N
Noise level = 1414.9330
Colorado
June 23, 1984
Radiometry
Period in minutes
50.0
12.5
7.1
5.0
3.8
3.1
2.6
2.3
2.0
300.0
240.0
180.0
120.0
60.0
0.0
Arbitrary units
0.00
0.06
0.12
0.18
0.24
0.30
0.36
0.42
0.48
Frequency, min-1

Fig. 7b

Maximum entropy method
M = 0.50 N
Noise level = 1414.9330
Colorado
June 23, 1984
Radiometry

Fig. 7c

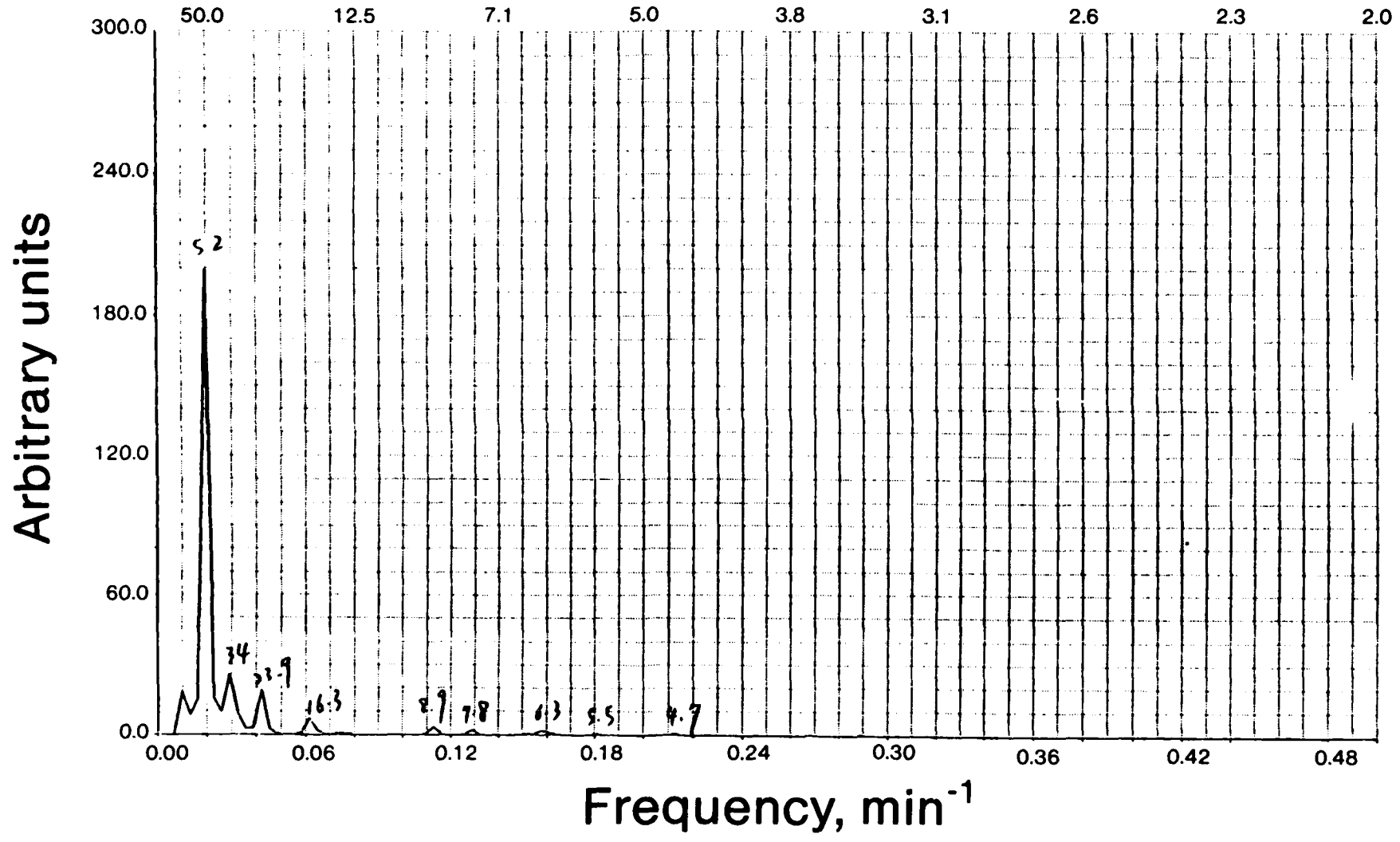

Data
Wyoming
June 29, 1984
OI 5577

Fig. 8a

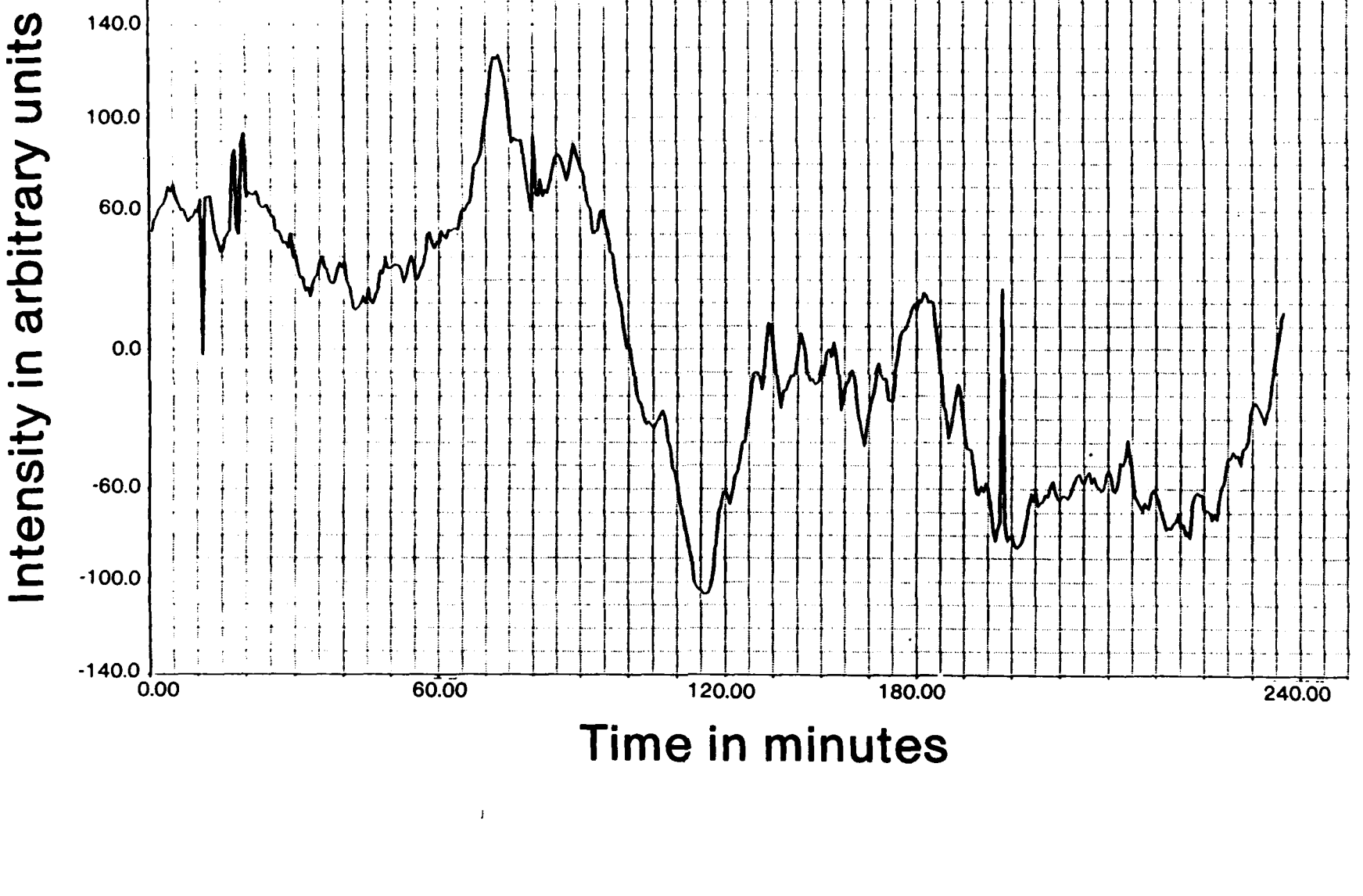

Maximum entropy method
M= 0.50 N
Noise level = 5295.8032
Wyoming
June 29, 1984
OI 5577

Fig 8b

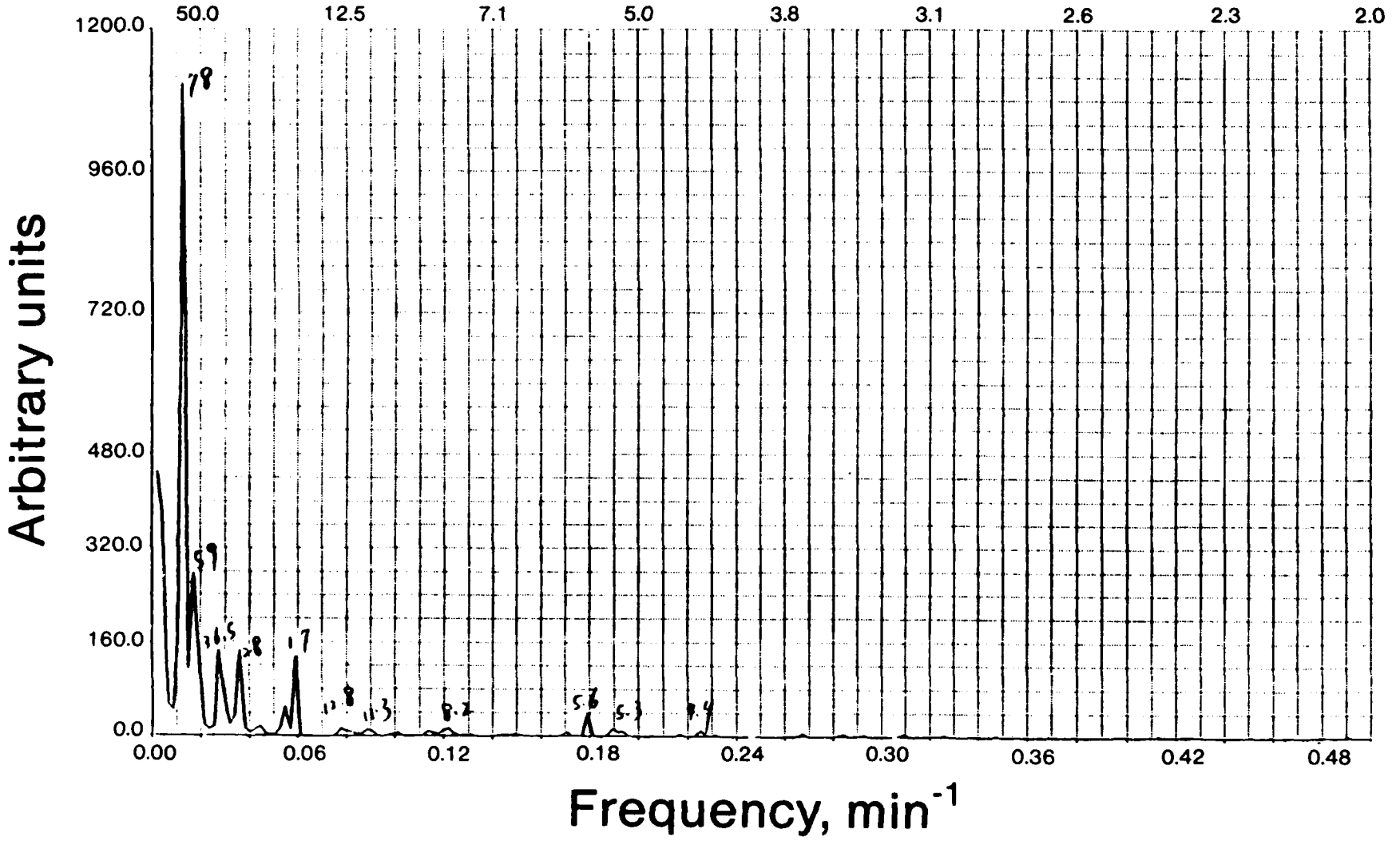

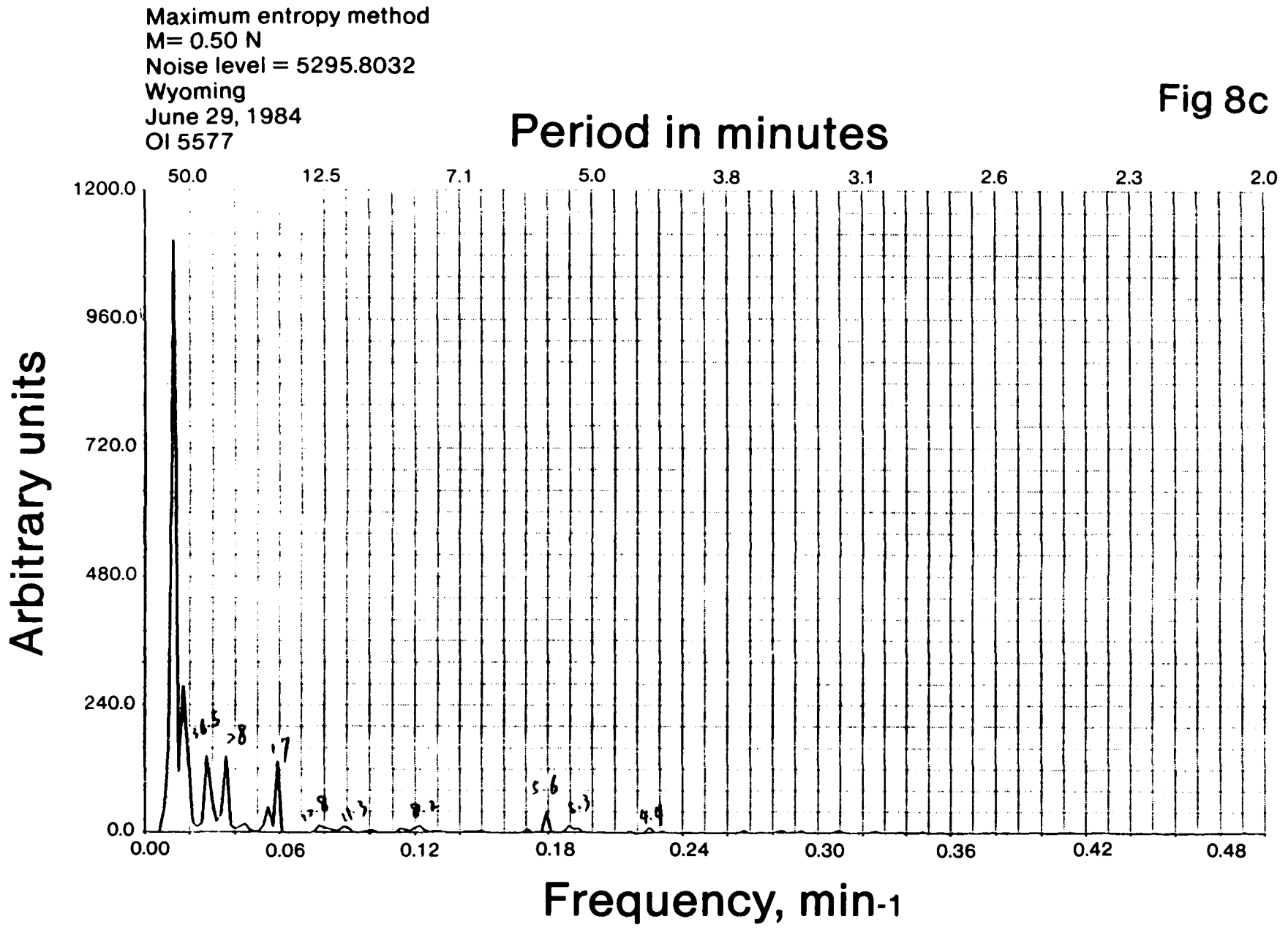
Maximum entropy method
M= 0.50 N
Noise level = 5295.8032
Wyoming
June 29, 1984
OI 5577
Fig 8c
Period in minutes
50.0
12.5
7.1
5.0
3.8
3.1
2.6
2.3
2.0
1200.0
960.0
720.0
480.0
240.0
0.0
Arbitrary units
16.5
>8
17
12.8
11.3
9.2
5.6
5.3
4.9
0.00
0.06
0.12
0.18
0.24
0.30
0.36
0.42
0.48
Frequency, min-1

Data
Wyoming
June 29 1984
OH 7900

Fig. 9a

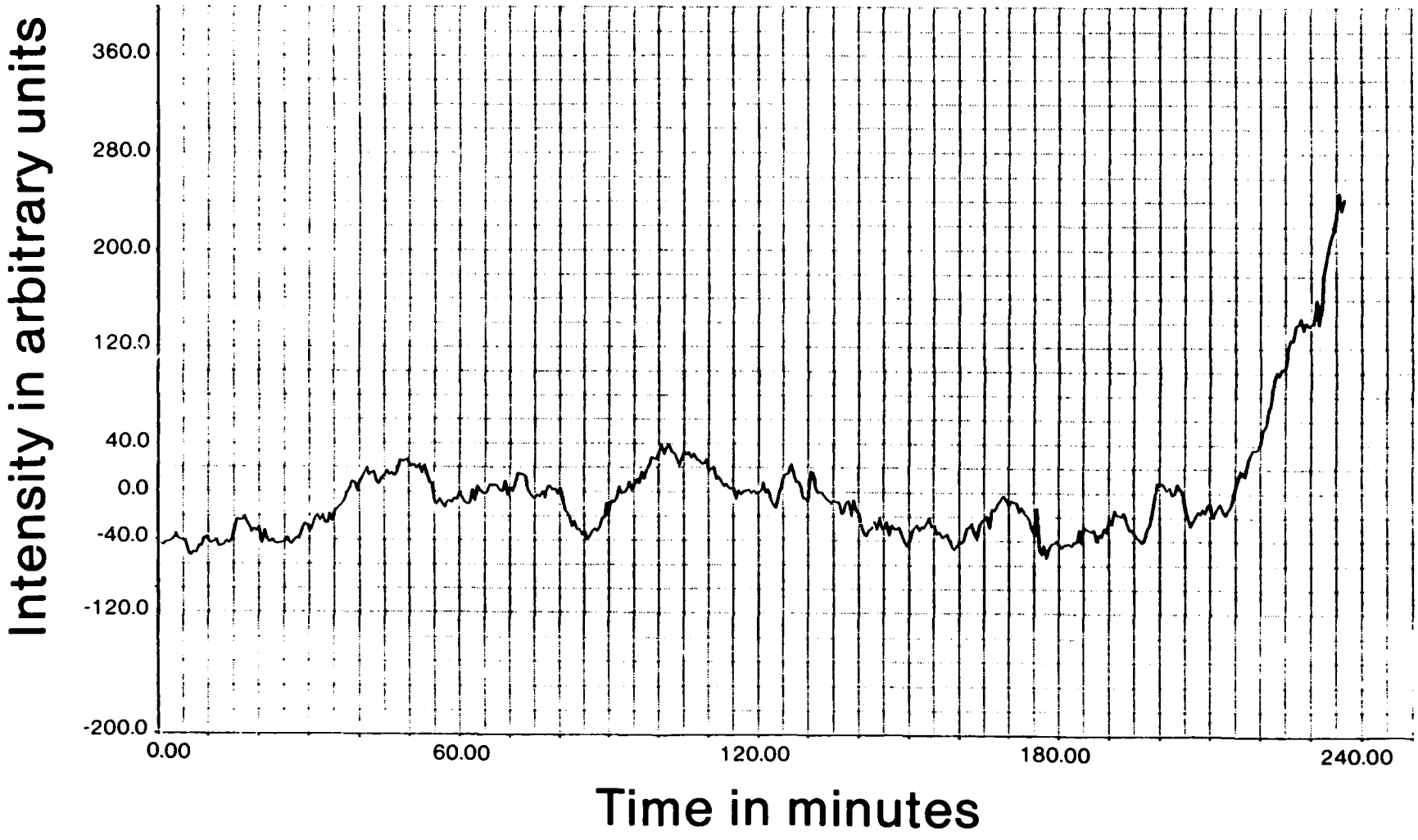

Maximum entropy method
M= 0.50 N
Noise level = 1915.0496
Wyoming
June 29, 1984
OH 7900

Fig. 9b

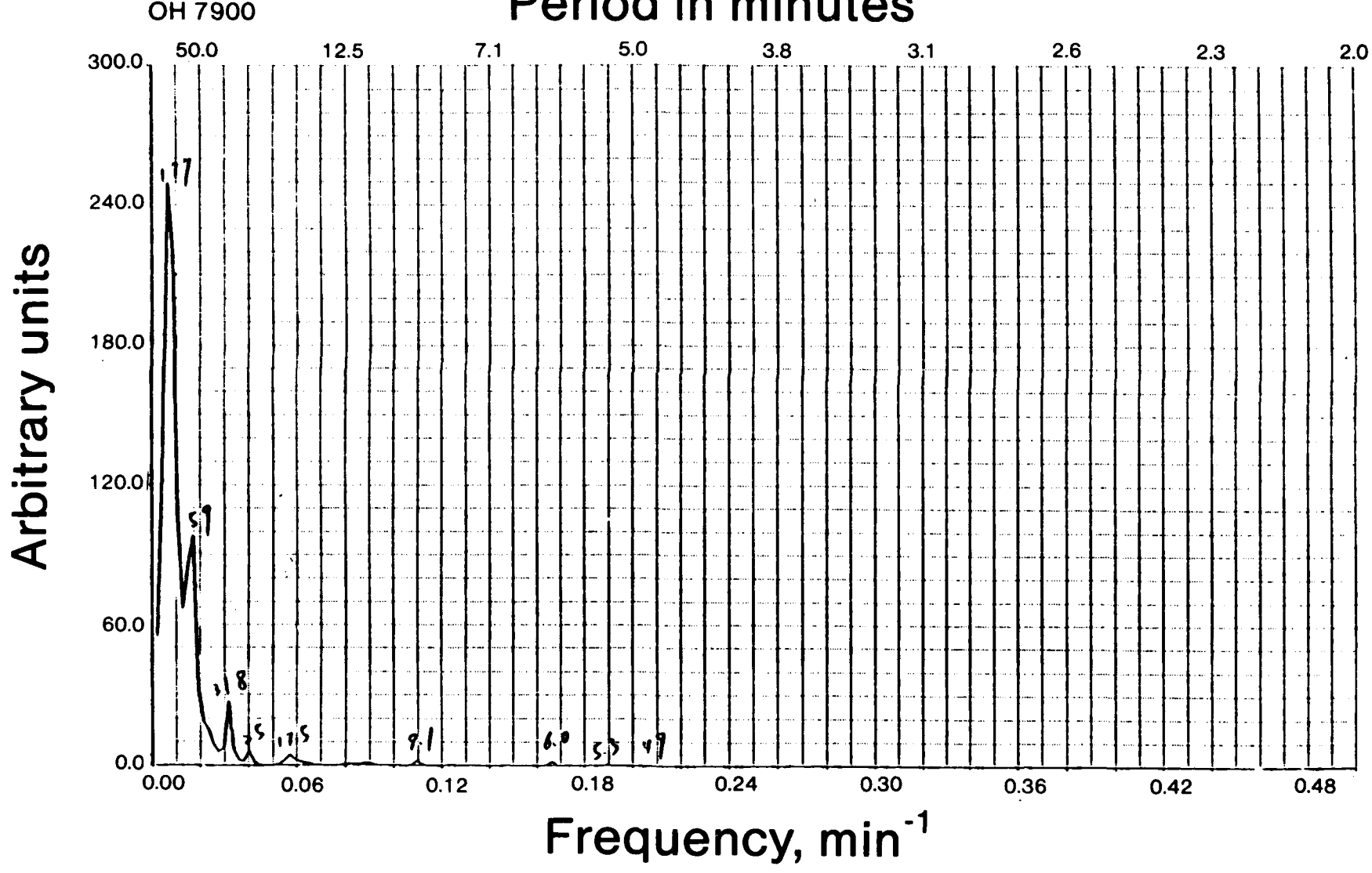

Maximum entropy method
M = 0.50 N
Noise level = 1915.0496
Wyoming
June 29, 1984
OH 7900

Fig. 9c

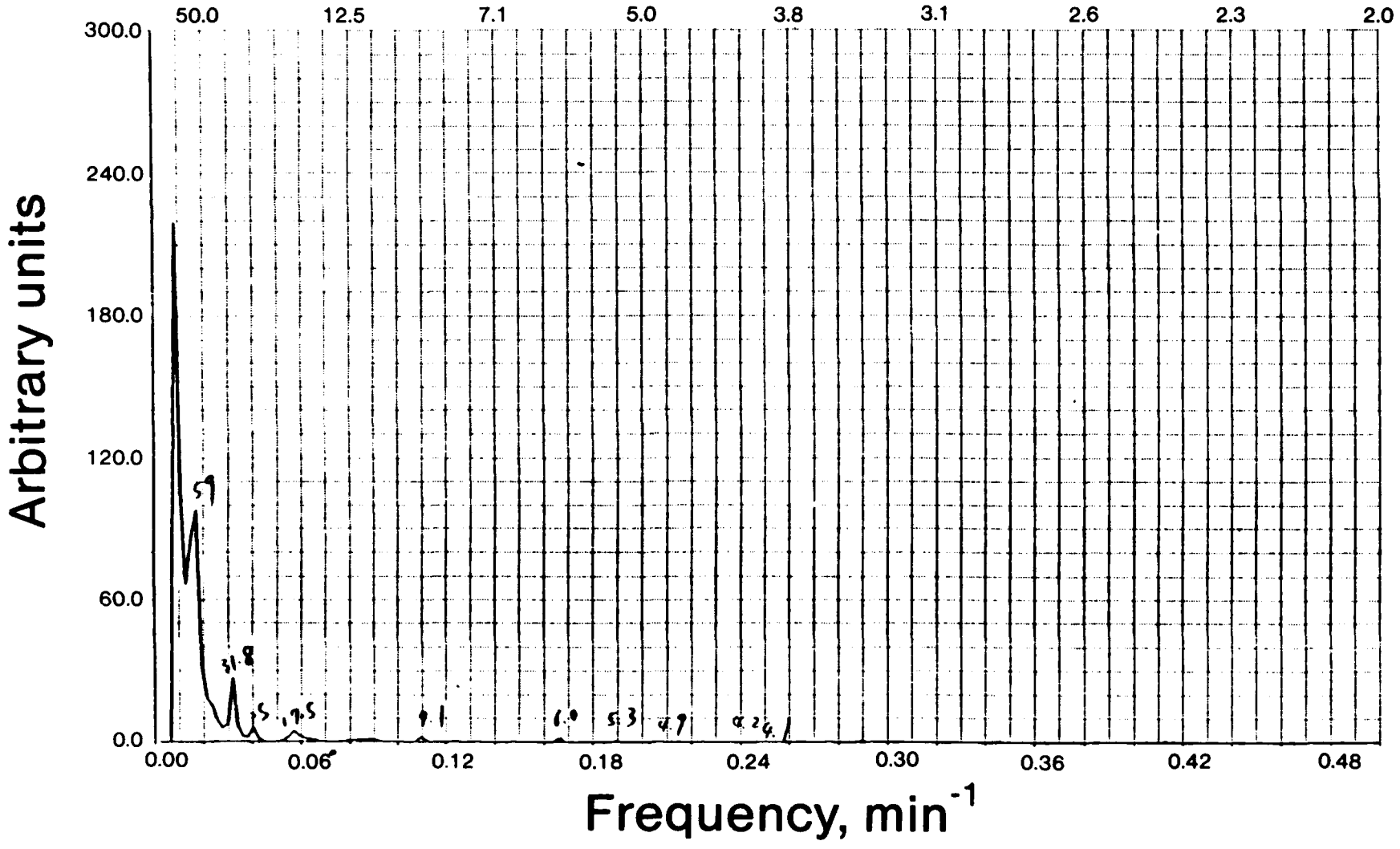

Data
New Mexico
June 29, 1984
OH 7300

Fig. 10a

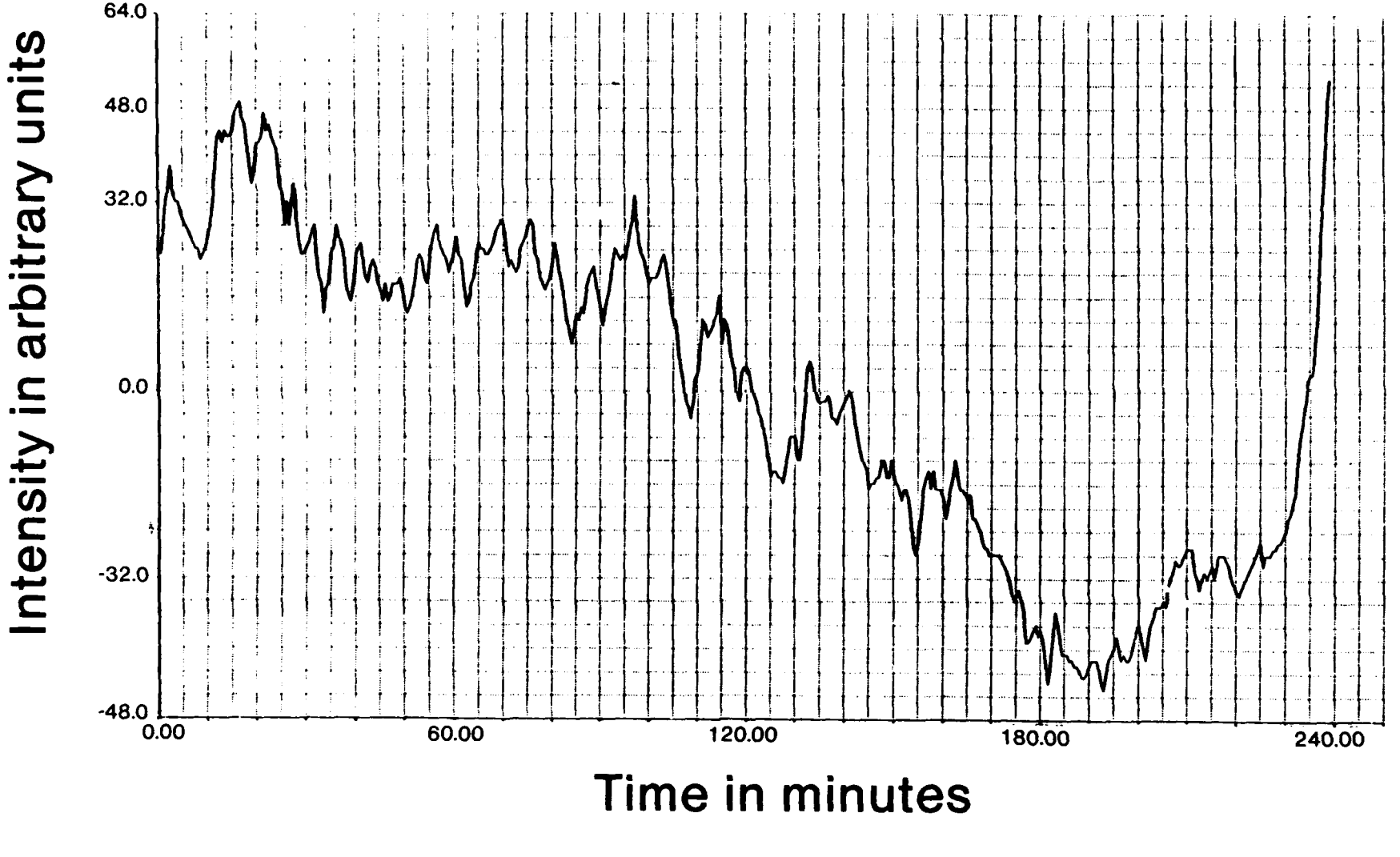

Maximum entropy method
M = 0.50 N
Noise level = 2.7059
New Mexico
June 29, 1984
OH 7300

Fig. 10b

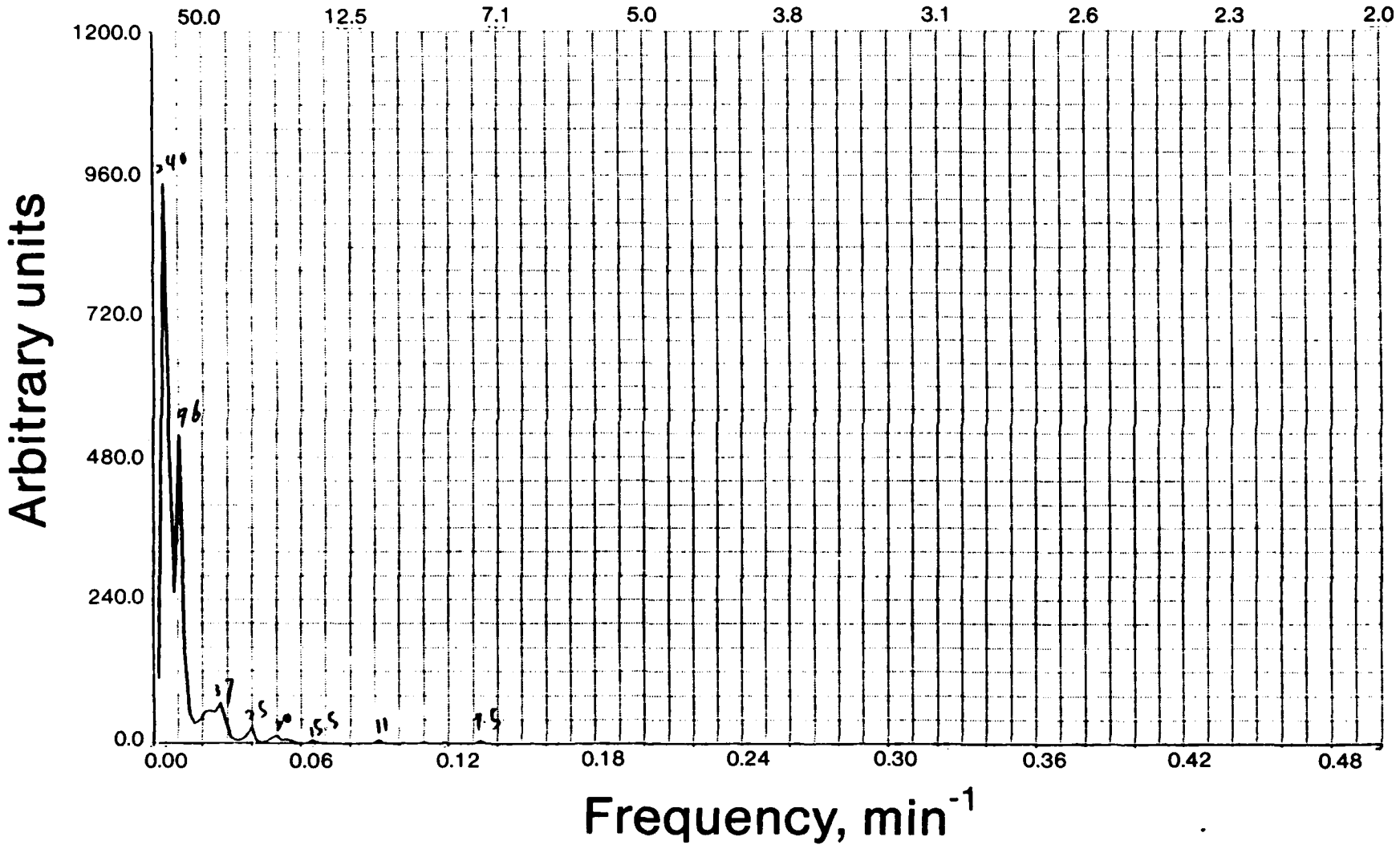

Maximum entropy method
M = 0.50 N
Noise level = 2.7059
New Mexico
June 29, 1984
OH 7300

Fig. 10c

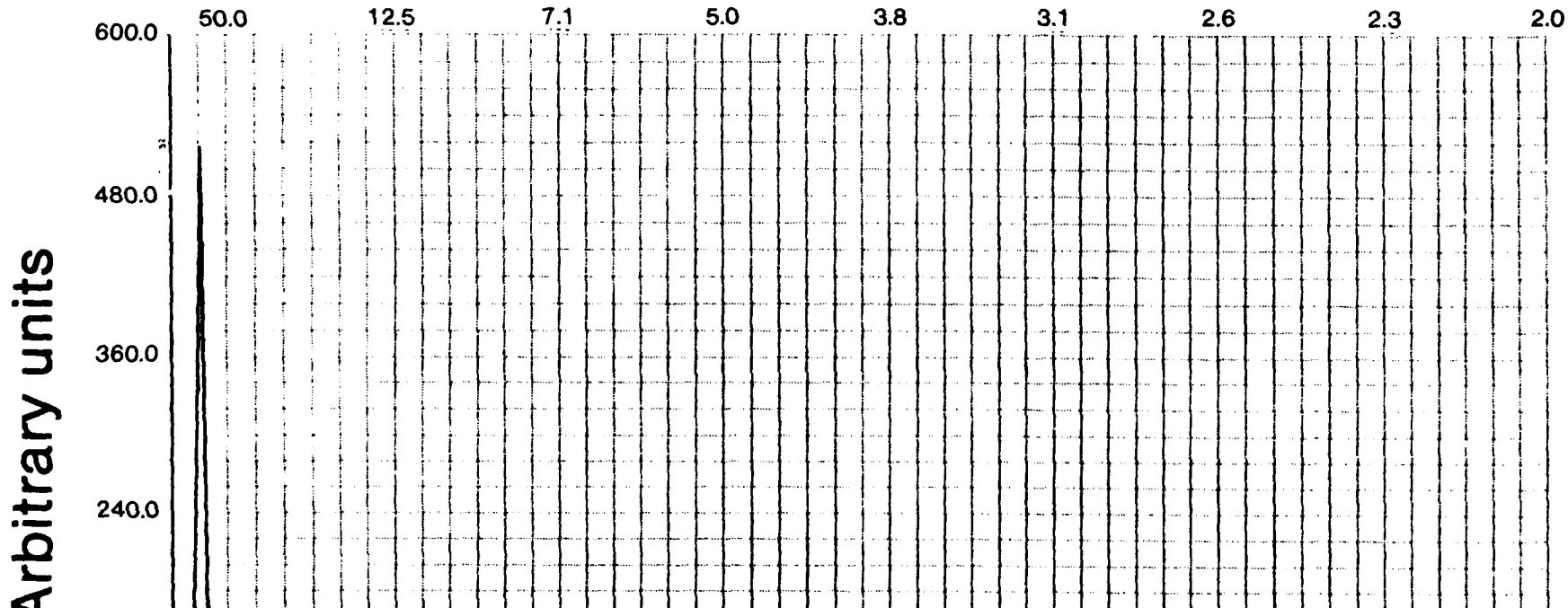

Data
Colorado
June 29, 1984
OI 5577

Fig. 11a

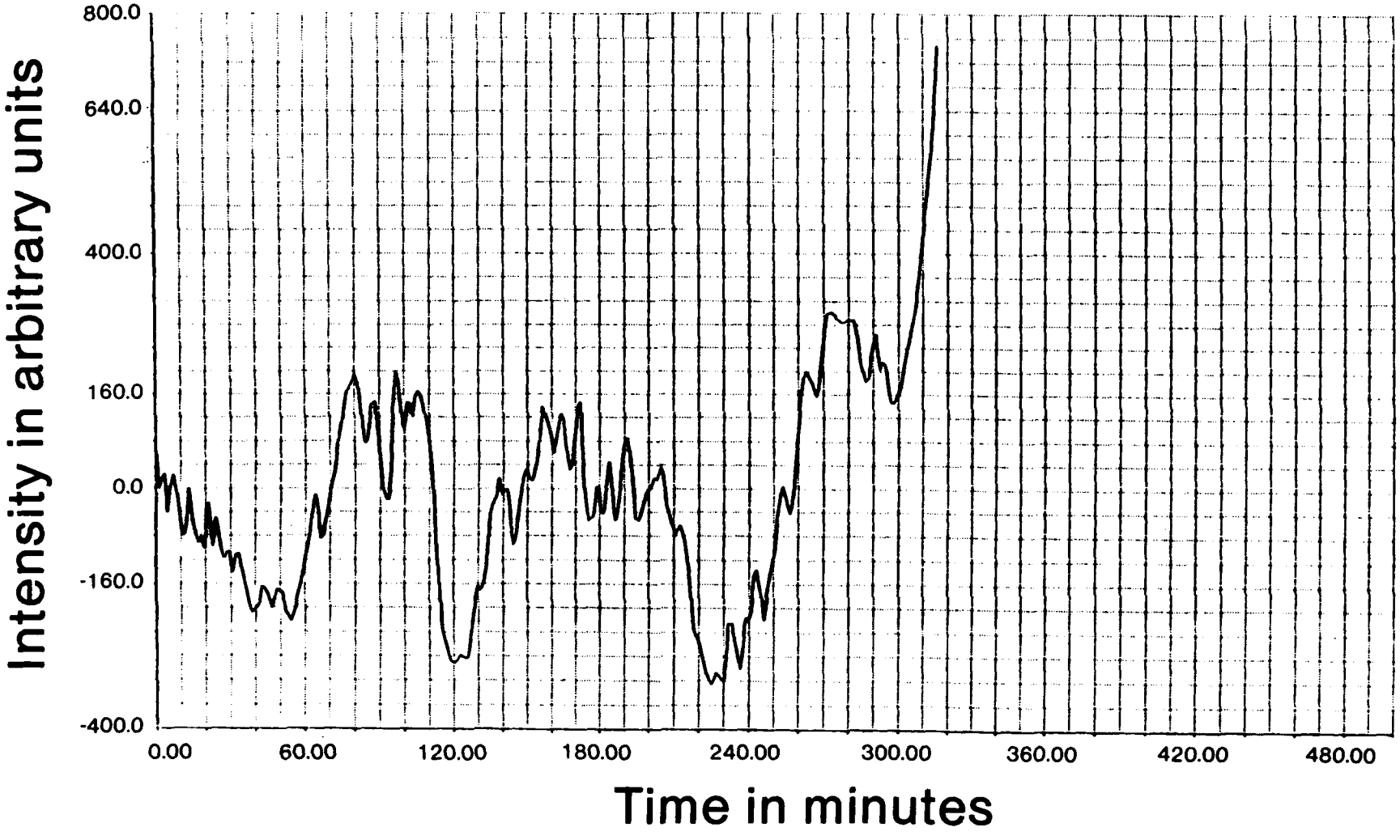

Maximum entropy method
M = 0.50 N
Noise level = 0.0065
Colorado
June 29, 1984
OI 5577

Fig. 11b

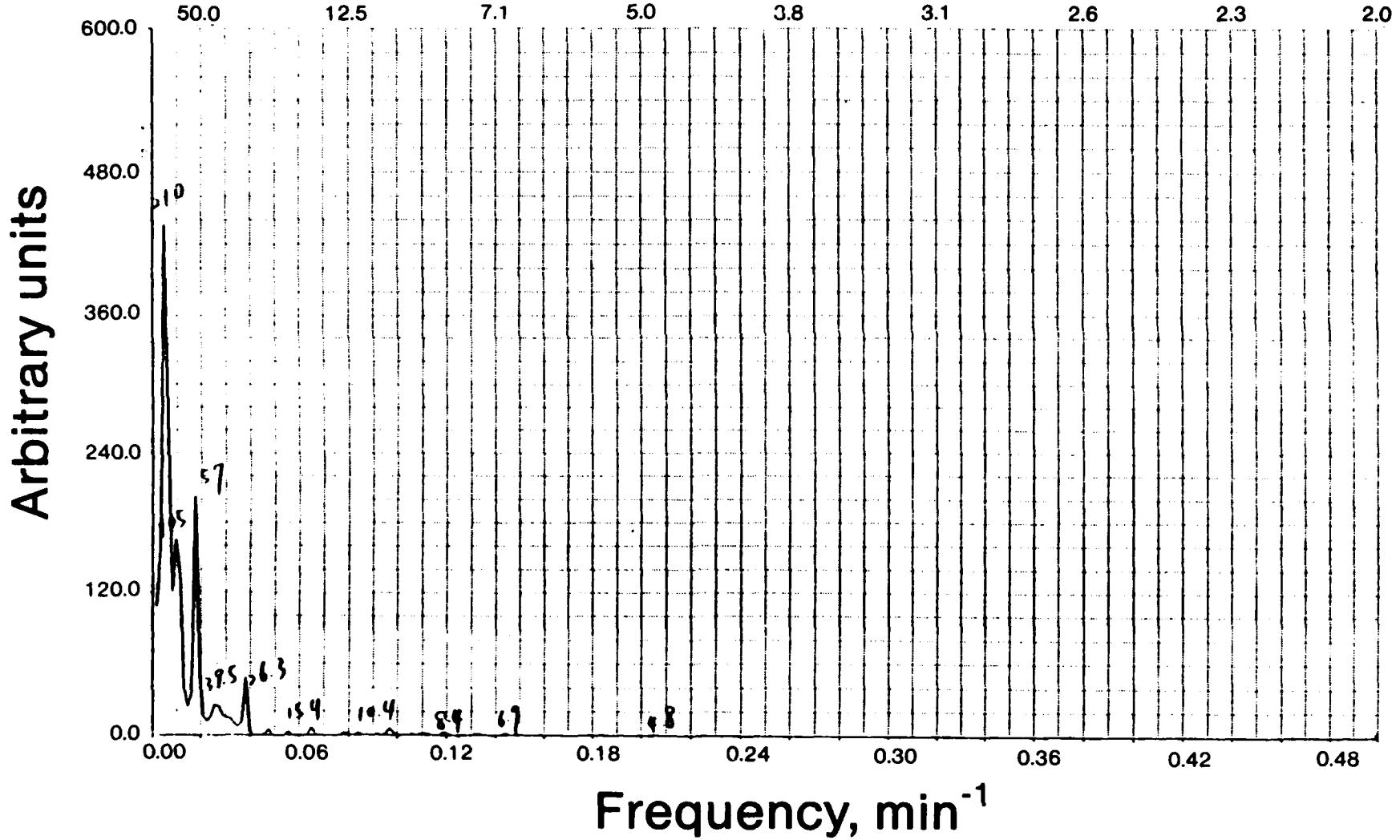

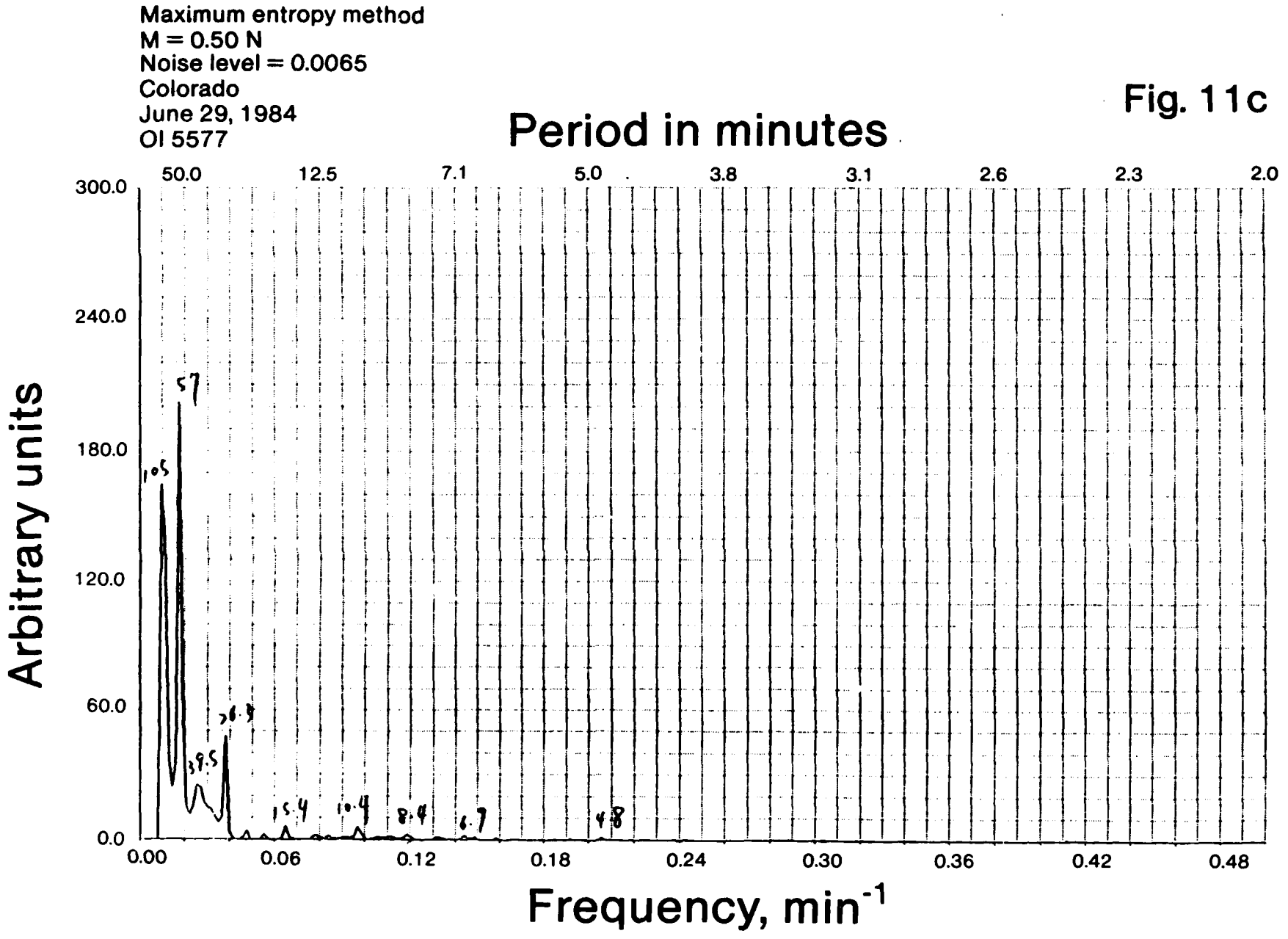
Maximum entropy method
M = 0.50 N
Noise level = 0.0065
Colorado
June 29, 1984
OI 5577
Period in minutes
50.0
12.5
7.1
5.0
3.8
3.1
2.6
2.3
2.0
300.0
240.0
180.0
120.0
60.0
0.0
Arbitrary units
57
10.5
39.5
26.9
15.4
10.4
8.4
6.7
4.8
0.00
0.06
0.12
0.18
0.24
0.30
0.36
0.42
0.48
Frequency, min-1

Fig. 11c

Data
Colorado
June 29, 1984
Radiometry

Fig. 12a

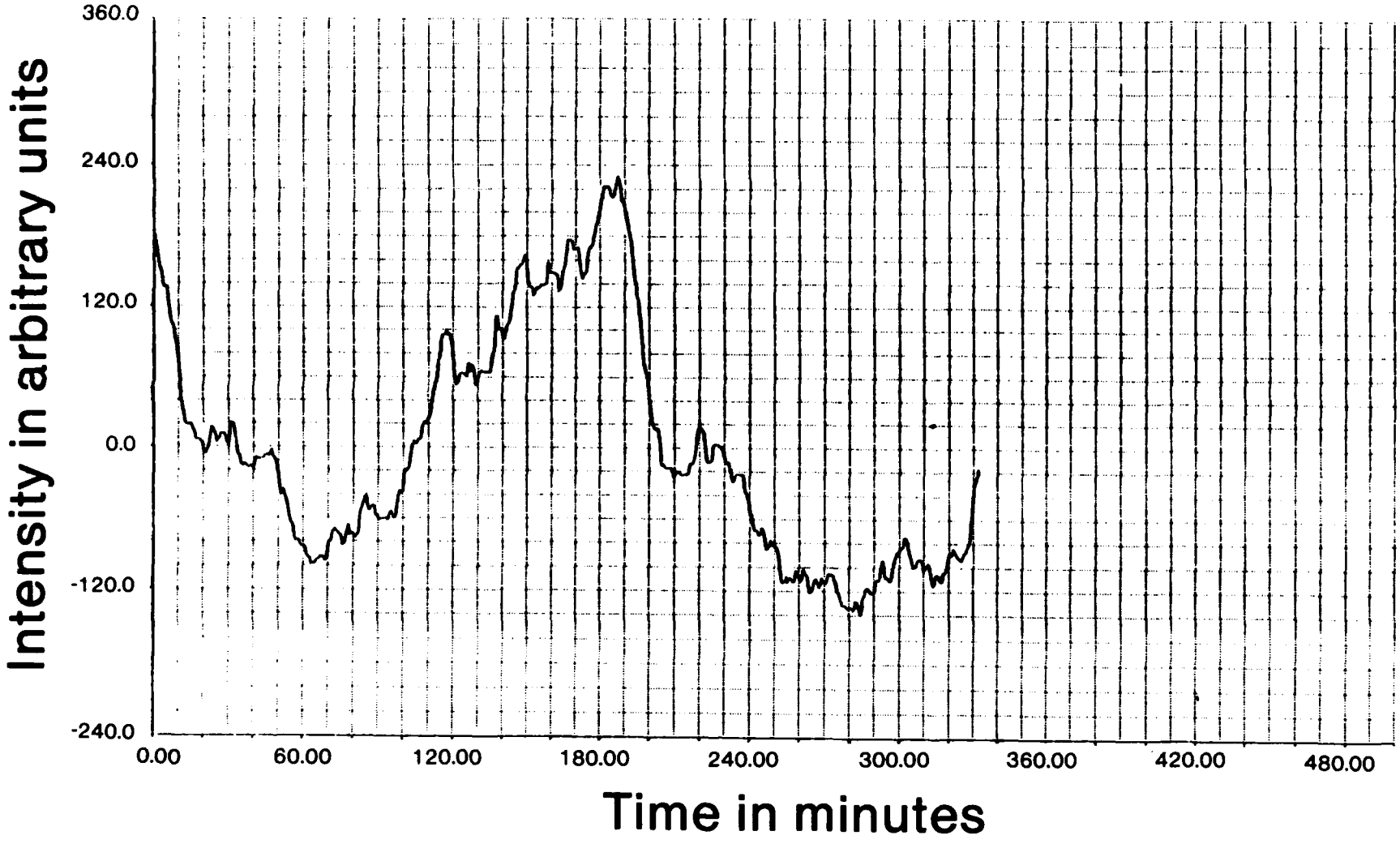

Maximum entropy method
M = 0.50 N
Noise level = 0.3305
Colorado
June 29, 1984
Radiometry

Fig. 12b

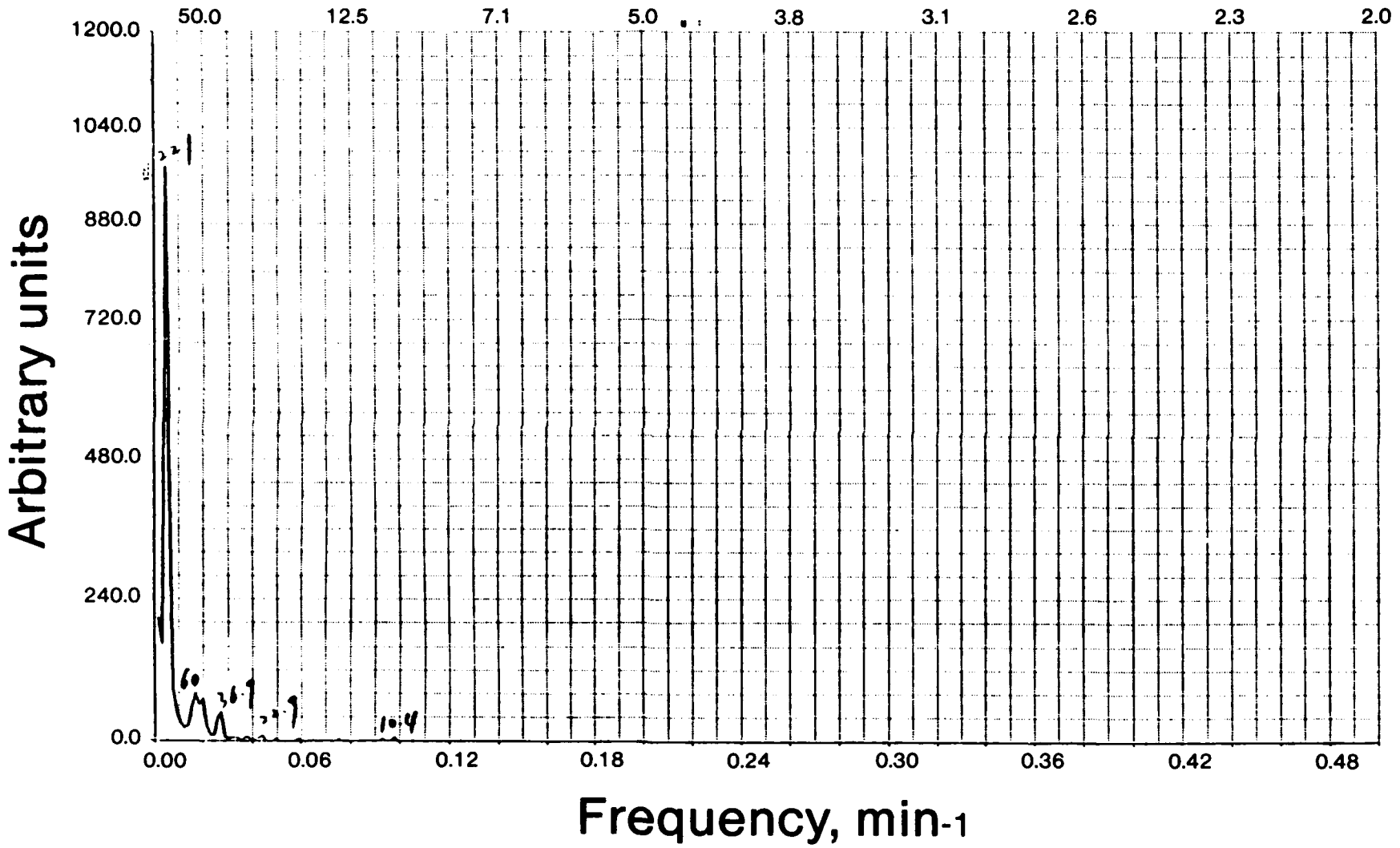

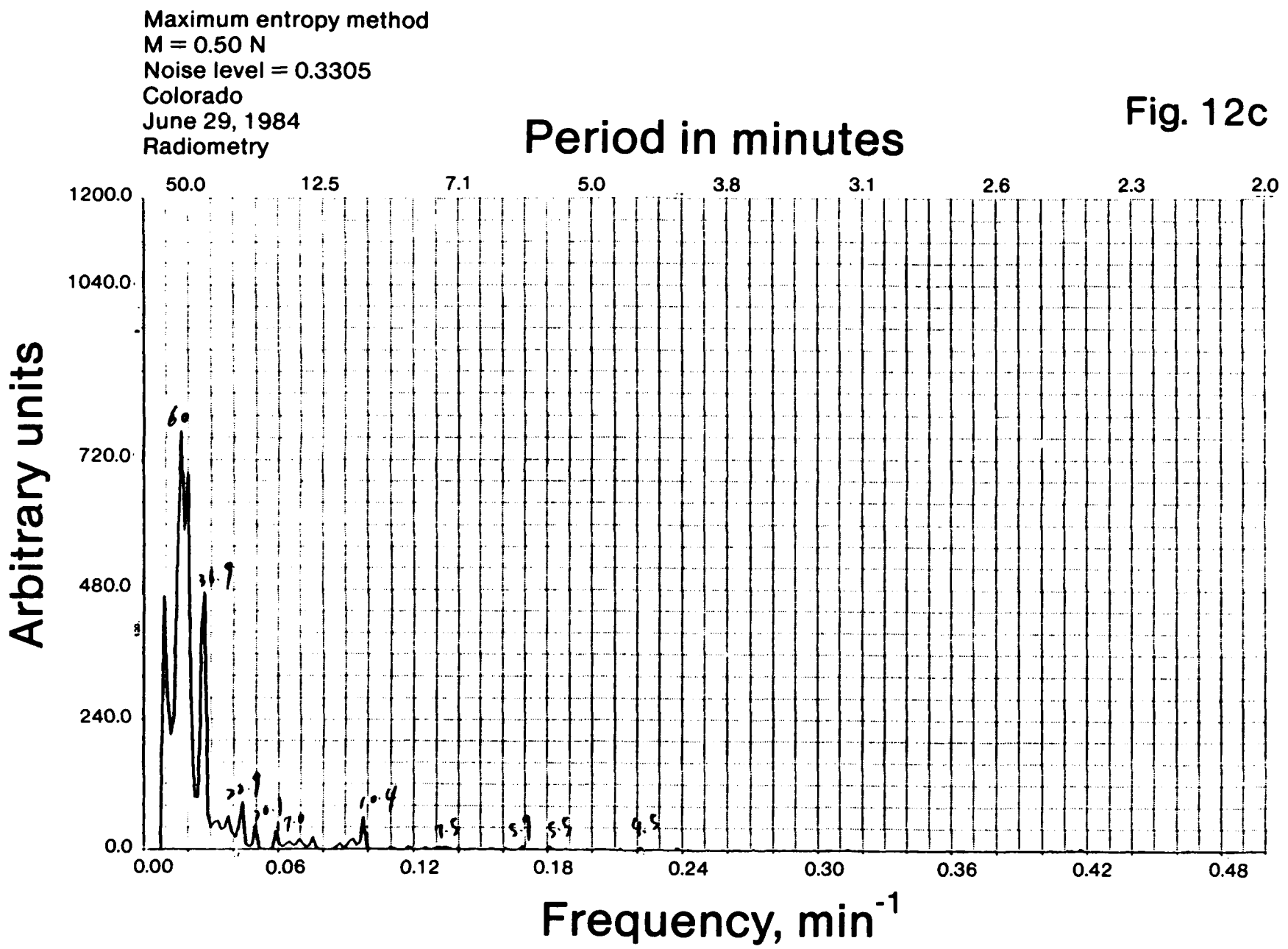
Maximum entropy method
M = 0.50 N
Noise level = 0.3305
Colorado
June 29, 1984
Radiometry
Period in minutes
50.0
12.5
7.1
5.0
3.8
3.1
2.6
2.3
2.0
1200.0
1040.0
720.0
480.0
240.0
0.0
Arbitrary units
0.00
0.06
0.12
0.18
0.24
0.30
0.36
0.42
0.48
Frequency, min-1

Fig. 12c

Fig. 13

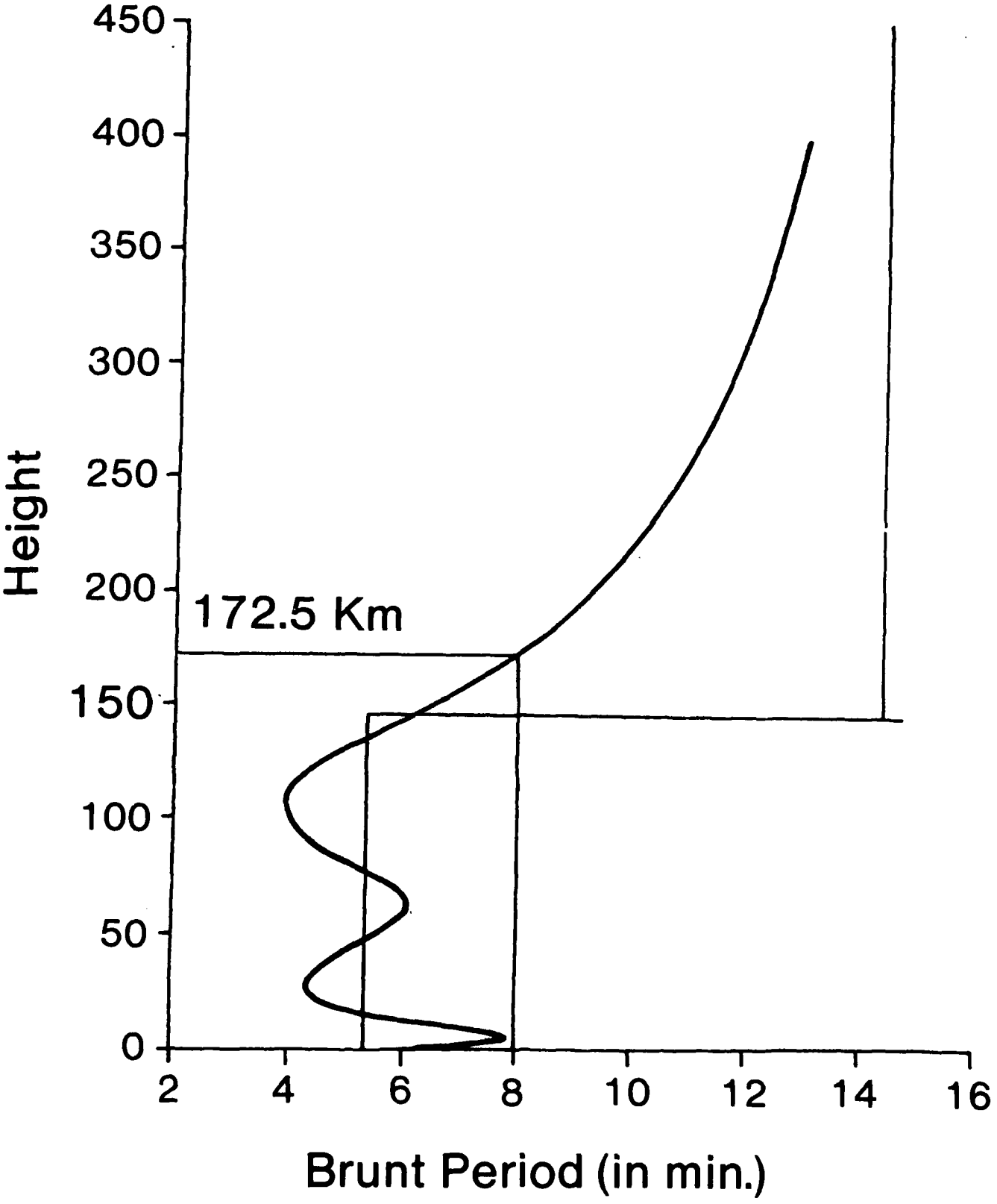
450
400
350
300
250
200
150
100
50
0
Height
172.5 Km
2
4
6
8
10
12
14
16
Brunt Period (in min.)

FIGURE 14

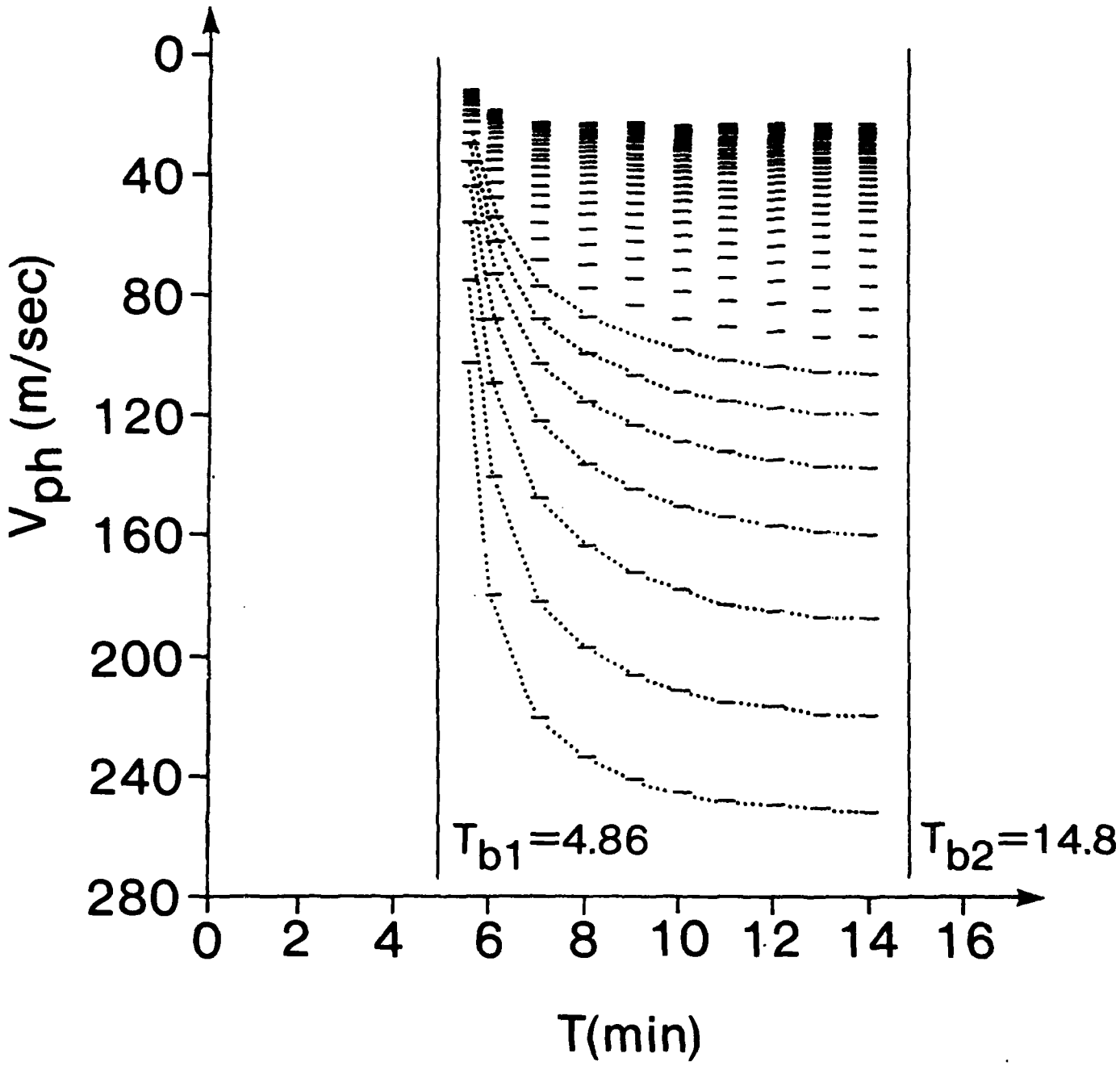
0
40
80
120
160
200
240
280
V_{ph} (m/sec)
T_{b1}=4.86
T_{b2}=14.8
0
2
4
6
8
10
12
14
16
T(min)

TABLE I

Common power spectrum peak

June 23,1984

	>30 min	20-30 min
Colorado OI 5577A	50, 36	21.5
Colorado Radiometry	52, 34	21.5
Wyoming OI 5577A		30, 21
Wyoming OH 7900A	38	26

TABLE II

Common power spectrum peak

June 29,1984

	>30 min	20-30 min
Colorado OI 5577A	57, 39.5	26.3, 21.8
Colorado Radiometry	60, 36.5	22.9, 20.1
Wyoming OI 5577A	59, 37	28
Wyoming OH 7900A	32	25
New Mexico OH 7300A	37	25

TABLE III

Common power spectrum peak

June 23,1984

	20-10 min
Colorado OI 5577A	15.8, 13.1, 12
Colorado Radiometry	16.6,
Wyoming OI 5577A	18, 16.6, 13, 11, 10.3
Wyoming OH 7900A	18, 14.2, 13.2, 12

TABLE IV

Common power spectrum peak

June 29,1984

	20-10 min
Colorado OI 5577A	18, 15.4, 12.9,11.9,10.4
Colorado Radiometry	17, 15.5,14.4,13.3,11.5,10.7,10.1
Wyoming OI 5577A	17, 12.8,11.3
Wyoming OH 7900A	18, 11.2
New Mexico OH 7300A	20, 15.5, 13.3,11.7

TABLE V

Common power spectrum peak

June 23,1984

	10-5 min
Colorado OI 5577A	10,8.5,9, 6.8,6.3, 5.6,5.2,4.6
Colorado Radiometry	8.9,7.8, 6.3, 5.5, 4.7
Wyoming OI 5577A	9.4, 7.6, 6.4,6.1,5.9,5.1
Wyoming OH 7900A	9.7,8.9,7.7,7.2 6.0, 5.4,4.8

TABLE VI

Common power spectrum peak

June 29,1984

	10-5 min
Colorado OI 5577A	8.4, 7.5,6.9,6.7,6.3,6.1, 5.4,5.2
Colorado Radiometry	8.5,8.0,7.7 5.9,5.5
Wyoming OI 5577A	8.2, 5.6,5.3
Wyoming OI 7900A	6.0, 5.3
New Mexico OI 7300A	8.4, 6.8, 5.8,5.5

TABLE VII

Percentage r.m.s.

	60 min			
	Colorado		Wyoming	
	OI	R	OI	OH
June 23, 1984	6.1	13.9	6.9	5.9
June 29, 1984	10.4	14.5	9.7	5.0
% based on Jn. 29	41	4.1	29	-18

	30 min			
	Colorado		Wyoming	
	OI	R	OI	OH
June 23, 1984	4.2	9.9	4.4	4.4
June 29, 1984	6.9	8.8	6.3	3.5
% based on Jn. 29	39	-13	31	-25

	15 min			
	Colorado		Wyoming	
	OI	R	OI	OH
June 23, 1984	3.0	6.0	3.3	2.9
June 29, 1984	4.7	5.1	4.4	2.8
% based on Jn. 29	37	-18	27	-1.4

TABLE VII (CONT)

	10 min			
	Colorado		Wyoming	
	OI	R	OI	OH
June 23, 1984	2.8	5.2	2.7	2.6
June 29, 1984	3.5	3.5	3.5	2.4
%based on June 29	19	-49	23	-8.8

	5 min			
	Colorado		Wyoming	
	OI	R	OI	OH
June 23, 1984	2.0	3.5	1.6	1.9
June 29, 1984	2.1	3.6	2.3	1.9
% based on Jn. 29	8.0	4.4	30	-0.5

TABLE VIII

Total average r.m.s. percentage

	Colorado		Wyoming	
	OI	R	OI	OH
June 23, 1984	14.7	15.5	13.0	9.16
June 29, 1984	13.2	27.1	15.1	5.70

TABLE IX

Average percentage r.m.s.

June 23, 1984		60 min	30 min
	Average r.m.s.	8.22	5.72
	% based on 60 min		69.6

June 23, 1984		15 min	10 min
	Average r.m.s.	3.78	3.34
	% based on 60 min	46.0	40.6

June 23, 1984		5 min
	Average r.m.s.	2.21
	% based on 60 min	26.9

TABLE IX (CONT)

June 29, 1984		60 min	30 min
	Average r.m.s.	9.918.	6.38
	% based on 60 min		64.4

June 29, 1984		15 min	10 min
	Average r.m.s.	4.26	3.23
	% based on 60 min	43.0	32.6

June 29, 1984		5 min
	Average r.m.s.	2.46
	% based on 60 min	24.8

TABLE X

Percentage r.m.s.

60 min		June 21	June 22	June 23
	OI 5577A	7.9	8.6	6.9
	OH 7900A	6.1	4.5	5.9
		June 27	June 28	June 29
	OI 5577A	11.6	6.8	9.7
	OH 7900A	8.0	3.8	5.0

30 min		June 21	June 22	June 23
	OI 5577A	7.9	8.6	6.9
	OH 7900A	6.1	4.5	5.9
		June 27	June 28	June 29
	OI 5577A	11.6	6.8	9.7
	OH 7900A	8.0	3.8	5.0

15 min		June 21	June 22	June 23
	OI 5577A	7.9	8.6	6.9
	OH 7900A	6.1	4.5	5.9
		June 27	June 28	June 29
	OI 5577A	11.6	6.8	9.7
	OH 7900A	8.0	3.8	5.0

TABLE X (CONT)

10 min		June 21	June 22	June 23
	OI 5577A	7.9	8.6	6.9
	OH 7900A	6.1	4.5	5.9
		June 27	June 28	June 29
	OI 5577A	11.6	6.8	9.7
	OH 7900A	8.0	3.8	5.0

5 min		June 21	June 22	June 23
	OI 5577A	7.9	8.6	6.9
	OH 7900A	6.1	4.5	5.9
		June 27	June 28	June 29
	OI 5577A	11.6	6.8	9.7
	OH 7900A	8.0	3.8	5.0

TABLE XI (a)

Construction of the horizontal velocity field at 90 km

June 23, 1984
Period = 150 min

V_{phx} (m sec^{-1})	$\alpha_k \cos k_x x_o$	$\alpha_k \sin k_x x_o$	$k_x x_o$	$\alpha_k \Delta U_s$ (m sec^{-1})
50	-8.48	-5.79	34.4°	-10.3
60	-3.55	-2.43	34.4°	-10.3
70	-9.11	-6.22	34.4°	-11.0
80	-6.28	-4.29	34.4°	-7.61
90	-3.86	-2.64	34.4°	-4.68
100	-3.48	-2.38	34.4°	-4.2
110	-3.64	-2.48	34.4°	-4.4
120	-4.78	-3.27	34.4°	-5.79
130	-3.36	-2.30	34.4°	-4.07
140	-1.90	-1.30	34.4°	-2.3
150	-5.85	-4.00	34.4°	-7.1

TABLE XI (b)

Construction of the horizontal velocity field at 90 km

June 23, 1984
Period = 37.5 min

V_{phx} (m sec^{-1})	$\alpha_k \cos k_x x_o$	$\alpha_k \sin k_x x_o$	$k_x x_o$	$\alpha_k \Delta U_s$ (m sec^{-1})
50	13.2	14.8	48.39	19.83
60	2.60	2.91	48.39	3.91
70	8.36	9.37	48.39	12.56
80	4.20	4.62	48.39	6.31
90	2.21	2.48	48.39	3.32
100	1.90	2.13	48.39	2.85
110	1.89	2.12	48.39	2.84
120	2.39	2.68	48.39	3.59
130	1.77	1.98	48.39	2.66
140	0.693	0.777	48.39	1.04
150	2.86	3.21	48.39	4.3

AD-A193 367 AN INVESTIGATION OF ATMOSPHERIC DYNAMICS THROUGH THEIR EFFECTS ON MESOSPH..(U) CINCINNATI UNIV OH DEPT OF PHYSICS T TUAN 23 MAR 87 AFGL-TR-87-0263 2/2

UNCLASSIFIED F19628-83-K-0026 F/G 4/1 NL

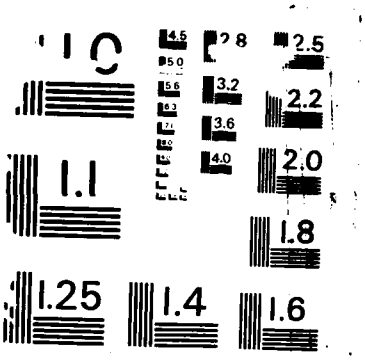

COPY RESOLUTION TEST CHART
NATIONAL BUREAU OF STANDARDS-1963-A

TABLE XI (c)

Construction of the horizontal velocity field at 90 km

June 29, 1984
Period = 70 min

V_{phx} (m sec^{-1})	$\alpha_k \cos k_x x_o$	$\alpha_k \sin k_x x_o$	$k_x x_o$	$\alpha_k \Delta U_s$ (m sec^{-1})
50	-2.01	-7.25	74.5	-7.5
60	-0.752	-2.71	74.5	-2.8
70	-1.95	-7.04	74.5	-7.3
80	-1.28	-4.60	74.5	-4.8
90	-0.774	-2.79	74.5	-2.9
100	-0.685	-2.47	74.5	-2.56
110	-0.707	-2.55	74.5	-2.65
120	-0.920	-3.31	74.5	-3.44
130	-0.640	-2.31	74.5	-2.4
140	-0.350	-1.26	74.5	-1.31
150	-1.12	-4.02	74.5	-4.2

TABLE XI (d)

Construction of the horizontal field at 90 km

June 29, 1984
Period = 19.1 min

V_{phx} (m sec^{-1})	$\alpha_k \cos k_x x_o$	$\alpha_k \sin k_x x_o$	$k_x x_o$	$\alpha_k \Delta U_s$ (m sec^{-1})
50	-0.315	0.962	-71.9^o	-1.01
60	1.95	-5.96	-71.9^o	6.27
70	-0.0733	0.224	-71.9^o	- .24
80	-0.132	0.404	-71.9^o	- .42
90	0.357	-1.09	-71.9^o	1.15
100	0.267	-0.816	-71.9^o	.86
110	0.234	-0.716	-71.9^o	.75
120	0.303	-0.927	-71.9^o	.97
130	0.240	-0.734	-71.9^o	.77
140	-1.87	4.90	-71.9^o	-6.01
150	0.321	-0.981	-71.9^o	1.03

END

DATE

FILMED

DTIC

JULY 88